NASA

Technical Memorandum 80598

Technique to Determine Location of Radio Sources from Measurements Taken on Spinning Spacecraft

J. Fainberg

NOVEMBER 1979

National Aeronautics and Space Administration

Goddard Space Flight Center
Greenbelt, Maryland 20771

TECHNIQUE TO DETERMINE LOCATION OF RADIO SOURCES FROM MEASUREMENTS TAKEN ON SPINNING SPACECRAFT

by

J.Fainberg
NASA/Goddard Space Flight Center
Laboratory for Extraterrestrial Physics
Greenbelt, MD 20771

November,1979

SUBMITTED TO RADIO SCIENCE

Abstract

The procedure developed to extract average source direction and average source size from spin-modulated radio astronomy data measured on the IMP-6 spacecraft is described. The method is quite general and fast and is easily implemented. Because all measurements are used, rather than just finding maxima or minima in the data, the method is very sensitive, even in the presence of large amounts of noise. The technique is applicable to all experiments with directivity characteristics. It is suitable for onboard processing on satellites to reduce the data flow to Earth. The application to spin-modulated non-polarized radio astronomy data is made in detail and includes the effects of noise, background, and second source interference. It is shown, for example, that measurements made using low-resolution dipole antennas with a sampling rate of about 2 measurements per spin period yield a determination of average source position with 1 deg accuracy for signals greater than several times background. This can be achieved utilizing only 25 samples from a receiver such as the Goddard Space Flight Center Radio Astronomy Experiment on IMP-6. For large sources such as solar bursts, the average source size can also be determined to a significant accuracy. In addition, the method permits the accurate restoration of the signal by removing the modulation. The analysis has been tested with computer simulated data and the results agree with analytic predictions. Applications of this method with IMP-6 radio data have led to a) determination of source positions of traveling solar radio bursts at large distances from the Sun, b) mapping of magnetospheric radio emissions by radio triangulation, and c) detection of low frequency radio emissions from Jupiter and Saturn.

1. INTRODUCTION

Many experimental measurements deal with physical quantities having a magnitude and direction (vector), such as fields (electric or magnetic) and fluxes (particle, photon). Most experiments are designed with a directivity (beamwidth) which is necessary for the determination of source direction and angular variation. Groundbased experiments emphasize narrow directivity and high sampling rate during an angular scan in order to resolve and measure sources of angular size comparable to the experiment beamwidth. However, for spacecraft measurements, the design of an experiment is greatly restricted by weight and power limitations. A narrow beamwidth for a given aperture size often implies reduced sensitivity; a high sampling rate to allow several samples per beamwidth requires a high telemetry bit rate. As a general rule, it is necessary that an experimenter not restrict beamwidth more than is required for the phenomena measured in order to conserve both experiment weight and telemetry resources.

In addition, there may be other factors affecting the measurement process which are even less under the experimenter's control. For example, the spin rate which determines how fast sources are scanned is a compromise between the needs of all experimenters and the requirements of spacecraft dynamics. In view of the conflicting requirements between spacecraft experiments and spacecraft operations, it becomes increasingly important to extract from the spacecraft data in an efficient way whatever information is present.

In this paper, we describe a data analysis technique developed for and first used with IMP-6 radio data (Fainberg et al,1972) which has applicability to a wide variety of spin modulated measurements. The technique is very fast, so that it is possible to process a large amount of data. It has great flexibilty

and sensitivity. In addition, with the source position and size determined, it is possible to accurately remove the effects of spin modulation and thereby determine the nature of the data in the absence of spin.

In Section 2, the analysis technique is discussed for general spin modulated experiments. In Section 3, the application of the analysis to spin modulated radio flux measurements is made in detail. Formulas are developed to account for effects of background, noise, and other sources on the measured source position and size. In Section 4 these techniques are applied to simulated radio bursts, with results agreeing quite well with analytic predictions. In addition, we show some examples of actual data processed from the IMP-6 spacecraft. Section 5 is concerned with future applications and extensions.

The purpose of this report is to discuss the data processing technique developed for the GSFC radio astronomy experiment on IMP-6, and to illustrate the technique with some applications to IMP-6 data. For an excellent review of low frequency satelite radio astronomy techniques in space, particularly with respect to questions of polarization , see Lecacheux et al [1979]. For a general review of spacecraft observations see also Steinberg [1979].

2. GENERAL METHOD

Initially we consider the case of a distant point source located in the spin plane of the experiment. Later we relax this restriction and show how an extended source out of the spin plane can be treated.

The spacecraft experiment has a normalized directive response or gain $G(\phi)$ which is a function of direction ϕ in the spin plane. For convenience we assume the maximum gain at $\phi = 0$, viz $G(0) = 1$. The gain function is determined by the design and calibration of the experiment. In all experiments, since $G(\phi)$

is periodic in ϕ (modulo 2π), it can be expressed as a Fourier series,

$$G(\phi) = \Sigma\ (b_k \cos k\phi + a_k \sin k\phi) \qquad (1)$$

where a_k and b_k are the Fourier coefficients obtained from $G(\phi)$ in the usual fashion. Very often symmetry considerations reduce the number of Fourier coefficients. For example, if the gain is symmetric about the direction of maximum gain, i.e. if $G(\phi) = G(-\phi)$, then $a_k = 0$ for all k, and

$$G(\phi) = \Sigma\ b_k \cos k\phi \qquad (2)$$

An example of a specific gain function is that of a dipole antenna with length short compared to radiation wavelength:

$$G(\phi) = \tfrac{1}{2}(1+\cos 2\phi) \qquad (3)$$

For antenna lengths comparable to wavelength, additional Fourier terms become significant. This case is treated in detail in Section 3.

For the general case let a distant small source of strength A be located at ϕ_s. Then the experiment response at time t will be

$$R(t) = G(\phi_s - \omega t + \omega t_0)A \qquad (4)$$

where

ω = spin angular velocity = 2π/spin period

t_0 = time when maximum gain is oriented in the reference direction (ϕ=0)

The source may be time varying in amplitude and position so that

$$R(t) = G(\phi_s(t) - \omega t + \omega t_0)A(t) \qquad (5)$$

where A(t) is the experiment response to the source at unity gain in the absence of spin. Since measurements are made at discrete times t_i, t_{i+1},..., the observed quantities form a time series $R(t_i)$, $R(t_{i+1})$,... The general problem we consider is the following: given this series of observable quantities $\{R(t_i)\}$ and the gain function of the experiment $G(\phi)$, how can we determine the source position and the source strength as functions of time, and what is the precision of the method taking into account noise, background, and the presence of other

sources?

The procedure we use is based on Fourier techniques in which we choose a processing window of N consecutive observations and form the sums C_1 and S_1 over N points where

$$C_1 = \Sigma\, R(t_i)\cos(\omega t_i - \omega t_0)$$
$$S_1 = \Sigma\, R(t_i)\sin(\omega t_i - \omega t_0) \qquad (6)$$

It is shown in Appendix A that these quantities reduce to

$$C_1 = \frac{1}{2} b_1\cos\phi_s + \frac{1}{2} a_1\sin\phi_s + \text{small terms}$$
$$S_1 = -\frac{1}{2} a_1\cos\phi_s + \frac{1}{2} b_1\sin\phi_s + \text{small terms} \qquad (7)$$

Therefore

$$\tan\phi_s = \frac{b_1 S_1 + a_1 C_1}{b_1 C_1 - a_1 S_1} \qquad (8)$$

The resulting source angle ϕ_s refers to the time of the midpoint of the processing window. The source angle at one sample time later can be obtained by shifting the times in Equations 6 by one sample time. (Note that this is easily done by adding one new term and subtracting one old term from the sums in Equations 6). In this way the evolution of source position ϕ_s with time can easily be calculated from experimental data.

Note that if the gain function (Equation 1) has significant Fourier terms of order k, then we also have

$$\tan k\phi_s = \frac{b_k S_k + a_k C_k}{b_k C_k - a_k S_k} \qquad (9)$$

where

$$C_k = \Sigma\, R(t_i)\cos k(\omega t_i - \omega t_0)$$
$$S_k = \Sigma\, R(t_i)\sin k(\omega t_i - \omega t_0) \qquad (10)$$

This allows an independent determination of source position utilizing each set of Fourier gain coefficients.

3. APPLICATION TO RADIO ASTRONOMY MEASUREMENTS

In this section we consider in detail the processing technique described in Section 2 applied to non-polarized radio data measured with a dipole antenna. In Section 3a the dipole gain function is discussed and the nature of the signal observed from a distant point source is introduced. In Section 3b we consider the effect of several point sources, discuss the response of point sources out of the spin plane, and then consider the case of a distributed source out of the spin plane. For these sources we introduce a quantity called the modulation index, specifying the amount of observed modulation. In Section 3c we give the procedure for determining the modulation index and source angle from the data. Section 3d is concerned with the accuracy of the source angle and modulation determination taking into account signal to noise ratio, effects of background, and the size of the processing window. In Section 3e we discuss the procedure for removing a modulated background from sporadic events.

3a. Dipole Gain Function

We consider the normalized gain function of a dipole antenna which spins about an axis perpendicular to the dipole elements. The angle ϕ is measured in the spin plane which also contains the dipole. (The case of a dipole not located in the spin plane will be treated in a subsequent paper). Angles are measured from the direction of maximum gain, which is the direction in the spin plane normal to the antenna elements. From Equation 2 we have

$$G(\phi) = \Sigma\, b_k \cos k\phi \qquad (11)$$

since $G(\phi) = G(-\phi)$. This antenna possesses another symmetry, $G(\phi) = G(\phi+180)$, which implies $b_k = 0$ for $k = 1,3,5,\ldots$ Therefore for a dipole the most general gain expansion is

$$G(\phi) = b_0 + b_2 \cos 2\phi + b_4 \cos 4\phi + \ldots \qquad (12)$$

For antennas short compared to the wavelength of the radiation measured, only the first two terms of this series are significant and

$$G(\phi) = \frac{1}{2} + \frac{1}{2}\cos 2\phi \qquad (13)$$

An expression for the gain of a dipole antenna which is not restricted to very short lengths is given by Jackson [1962]:

$$G(\phi) = G_0 \left[\cos\tfrac{1}{2}(kd\sin\phi) - \cos\tfrac{1}{2}kd \right]^2 / \cos^2\phi \qquad (14)$$

where

$k = 2\pi/\lambda$

λ = wavelength of radiation

d = total length of antenna

$G_0 = [1-\cos\tfrac{1}{2}kd]^{-2}$

Note that this reduces to Equation 3 for $kd \ll 1$.

We can expand this general dipole gain function in the form of Equation 12 by standard Fourier techniques. We have done this by numerical integration and have plotted the coefficients b_0, b_2, b_4, and b_6 in Figure 1 as a function of normalized antenna length. It is clear that Equation 13 is an accurate representation for the gain for wavelengths larger than half the dipole length. For shorter wavelengths the terms b_4, b_6, etc may be large enough to be useful in the procedure given in Equation 9.

3b. Nature of Observed Signals

To illustrate the development of the techniques in detail, we consider the range of situations where Equation 3 is sufficient. In most of the development it is possible to generalize the treatment to include the higher Fourier terms and to include corrections for $b_2/b_0 \neq 1$.

For the short dipole the observed signal from a distant point source in the spin plane is given by Equations 5 and 3,

$$R(t) = \frac{1}{2}[1+\cos 2(\omega t-\phi_s)]A(t) \qquad (15)$$

where A(t) is the signal observed by a unity gain antenna in the absence of spin. For most cases of interest A(t) and $\phi_s(t)$ are slowly varying functions compared to $\cos 2\omega t$. These cases are illustrated in examples in Section 4 where the spin modulation is rapid compared to the slower variations in actual data. When A(t) has more rapid time structure the effect will be seen to be somewhat equivalent to a poorer signal to noise ratio in the determination of ϕ using the techniques proposed. We write Equation 15 in the form

$$R(t) = [1+ \cos 2(\omega t-\phi_1)]A_1 \qquad (16)$$

keeping in mind that source strength A_1 (which now includes a factor of $\frac{1}{2}$) and source direction ϕ_1 may be slowly varying in times.

In the remainder of this section we will show that any distribution of sources results in an observed signal of the form

$$R(t) = [1+ \alpha \cos 2(\omega t-\phi)]A \qquad (17)$$

where A is a measure of the amplitude of the source, ϕ is the arrival direction of the midpoint of the source projected onto the spin plane, and α is defined as the modulation index such that $0 \leq \alpha \leq 1$. To show this we consider 3 cases: two point sources located in the plane of spin; one point source located out of the spin plane; and a uniformly distributed conical source.

Case 1

For two point sources located at ϕ_1 and ϕ_2 we have for the observed signal

$$R_T(t) = R_1(t)+R_2(t) \qquad (18)$$

where $R_1(t)$ and $R_2(t)$ are given by Equation 16. By standard trigonometric procedure it is possible to write this in the form

$$R_T(t) = [1+\alpha_T \cos 2(\omega t-\phi_T)]A_T \qquad (19)$$

where ϕ_T is a source angle representing a weighted mean of ϕ_1 and ϕ_2, and A_T is the sum of the individual source strenths A_1 and A_2.

Here $\alpha_T \leq 1$ and is a positive quantity which we define as the modulation index. When the two point sources are in the same (or opposite) direction, $\alpha_T=1$. When two equal sources are at 90°, $\alpha_T=0$ (no modulation). The modulation index is than a measure of the separation of the two sources. Rather than giving detailed expressions for α_T and ϕ_T for two point sources now we defer this until later in this section when we consider the sum of two point sources not restricted to the spin plane.

Case 2

We consider a point source located out of the spin plane. It is clear that we cannot have $\alpha = 1$ because the observed intensity R(t) can never be zero since the null of the antenna no longer passes through the entire source. This case is treated exactly in Appendix B and we again can express the result in the form of Equation 17 where ϕ is the azimuthal angle of the source in the spin plane and the moduation index is given by

$$\alpha = \sin^2\theta/(2-\sin^2\theta) \qquad (20)$$

where θ is the angle of the point source to the spin axis. We note that here again the modulation index is between 0 and 1. However, lack of full modulation in this case is due to a point source out of the spin plane.

The modulation index α is a quantity which we can determine along with source

direction from the observed data. However, it is clear that a unique conclusion from α is not possible; lack of complete modulation can be due either to a point source out of the spin plane or to distributed sources. The range of ambiguity is restricted, however, and the modulation index does contain important information. We can explore this aspect by treating next a very general case: that of a distributed uniform source centered out of the spin plane.

Case 3

We consider a uniform conical source of angular width γ, located with its axis inclined to the spin axis at an arbitrary angle θ. The signal observed from this source has been expressed in closed form in Appendix B. We find that

$$R_T = [1+\alpha\cos 2(\omega t-\phi)]A \qquad (21)$$

where the modulation index is given by

$$\alpha = \sin^2\theta/(K-\sin^2\theta) \qquad (22)$$

where

$$K = [8+2\cos\gamma(1+\cos\gamma)]/[3\cos\gamma(1+\cos\gamma)]$$

γ= half total angular width of cone

We note that for $\theta = 90^\circ$ and for $\gamma = 0$ this expression describes the case of a point source in the spin plane ($\alpha = 1$). For $\gamma = 0$ this case refers to a point source out of the spin plane, and Equation 22 reduces to Equation 20.

For a given α, only a certain range of source widths and source inclinations is possible. Figure 2 presents a graphic description of this range for various values of α derived from Equation 22. In this figure the vertical axis represents the elevation of the source from the spin plane. The horizontal scale is half the total width of the uniform conical source. Once a value of modulation index is found the allowed range of source widths and source inclinations is given by the appropriate curve in Figure 2. The closer the modulation index is to unity the less the range of ambiguity.

3c Dipole Results

We start with the most general form of observed signal from a short dipole antenna located in the spin plane, including now an unmodulated background B,

$$R(t) = [1+\alpha\cos 2(\omega t-\phi)]A + B \qquad (23)$$

where $R(t)$ is observed only at discrete times t_i. We wish to determine from $\{R(t_i)\}$ alone the quantities α, ϕ, and A which, in general, are slowly varying in time compared to the modulation imposed by the spin. We assume B can be determined at a time when the source is not present. Following the procedure of Section 2 we form the sums

$$C_2 = \Sigma\, R(t_i)\cos 2\omega t_i$$

$$S_2 = \Sigma\, R(t_i)\sin 2\omega t_i \qquad (24)$$

and also

$$C_0 = \Sigma\, R(t_i)$$

where $\omega = 2\pi/\text{spin period}$.

In order to explore the meaning of S_2, C_2, and C_0, we will assume Equation 23 and insert this in Equations 24 in order to find expressions for α, ϕ, and A in terms of the observed data $\{R(t_i)\}$ only. In addition, it is important to note that A and B are noise quantities that are sampled by an instrument with certain physical parameters. It can be shown (Kraus,1966) that the rms fluctuation ΔA resulting from a radiometer measuring a noise signal of average power A is

$$\Delta A = A/\sqrt{(\beta\tau)} \qquad (25)$$

where β is the predetection bandwidth of the radiometer and τ is the post-detection integration time. Similarly

$$\Delta B = B/\sqrt{(\beta\tau)} \qquad (26)$$

where ΔB is the rms fluctuation in the measured background power B. Using Equations 13 and 14 we find (Appendix A) that

$$S_2 = \tfrac{1}{2}N\alpha A\sin 2\phi \pm O(\Delta S_2)$$
$$C_2 = \tfrac{1}{2}N\alpha A\cos 2\phi \pm O(\Delta C_2) \qquad (27)$$
$$C_0 = NA+NB \pm O(\Delta C_0)$$

where $O(\Delta S_2)$, $O(\Delta S_2)$, and $O(\Delta C_0)$ are small terms of the order of the standard deviations. Neglecting the small terms, Equations 27 can be solved for α, ϕ, and A:

$$\tan 2\phi = S_2/C_2 \qquad (28)$$
$$\alpha = 2\sqrt{[S_2^2+C_2^2]}/[C_0-NB] \qquad (29)$$

or finally

$$\tan 2\phi = \frac{\Sigma\, R(t_i)\sin 2\omega t_i}{\Sigma\, R(t_i)\cos 2\omega t_i}$$
$$\alpha = 2\sqrt{[(\Sigma\, R(t_i)\sin 2\omega t_i)^2+(\Sigma\, R(t_i)\sin 2\omega t_i)^2]}/\Sigma\,[R(t_i)-B] \qquad (30)$$
$$A = \tfrac{1}{N}\Sigma\,[R(t_i)-B]$$

which expresses the desired quantities in terms of the observables $R(t_i)$ and the spin period. We note that Equation 30 is a special case of the general solution given in Equations 9.

To reconstruct the signal that would be observed by an antenna with no spin there are two possible approaches. One method is to use Equations 30 and multiply by $(1+\alpha)$ in order to insure the appropriate normalization

$$A(t_{N/2}) = \tfrac{1}{N}(1+\alpha)\Sigma\,[R(t_i)-B] \qquad (31)$$

This is quite useful but it does involve a smoothing over the window length of N samples. Another method is to use Equation 17 which yields

$$A_0(t_i) = (1+\alpha)[R(t_i)-B]/[1+\alpha\cos 2(\omega t_i-\phi)] \qquad (32)$$

where α and ϕ are determined in Equations 30. This function, which we call the despun function, does not involve a smoothing of A(t) over the window (except for the determination of α and ϕ) and more accurately follows variations with time, but at the expense of more noise. In the next section we consider how the

accuracies of ϕ, α, and A are affected by the error terms in Equations 27.

3d. Accuracy of Method: Unmodulated Background

We consider first the error in ϕ due to the terms ΔS_2 and ΔC_2. If ΔA and ΔB are the rms fluctuations of signal and background respectively, and $\Delta\phi$ and $\Delta\alpha$ are the rms values of errors in ϕ and α respectively, we have shown in Appendix A

$$\Delta\phi_s = \frac{1}{\alpha}\sqrt{[1+\tfrac{1}{4}\alpha^2+(1+\alpha)^2\ \Delta A^2/\Delta B^2]}\,\Delta A/[A\sqrt{(2N)}] \text{ radians}$$

Using Equations 25 and 26 we get

$$\Delta\phi_s = \frac{1}{\alpha}\sqrt{[1+\tfrac{1}{4}\alpha^2+(1+\alpha)^2\ A^2/B^2]}/[\sqrt{(2N\beta\tau)}] \text{ radians} \qquad (33)$$

For large A/B

$$\Delta\alpha = \sqrt{[2-3\alpha^2/2+\alpha^4/2]}/\sqrt{(N\beta\tau)} \qquad (34)$$

Several implications of these results are clear. Once the signal to background ratio A/B is greater than about 5, the background has a small effect on the accuracy of ϕ. On the other hand, if the signal A is long lasting, one can reduce the errors in ϕ and α by increasing N, which is effective even for very poor signal to noise ratios.

Consider the case where A/B = 5 and $1/\sqrt{(\beta\tau)} = 0.09$ (value of $\beta\tau$ for the GSFC radiometer on IMP-6). Then for N= 25, $\Delta\phi \approx$ 1 deg and $\delta\alpha \approx 0.02$. This indicates the great sensitivity of this data processing method.

There are several considerations governing the choice of N. Large processing windows decrease errors by $1/\sqrt{N}$. However, they also smooth out structure within the time period of N samples. This effect is very similar to the use of a rejection filter to get rid of noise signals, but at the expense of losing signal components within the same frequency range. Another consideration is that the number of samples N be such that an even sampling of phases occurs in

the sums for appropriate cancellation. We have achieved good results with N as small as 12. Very often there is an aliasing between the sampling time and the spin rate. This occurs when the sampling time is such that the detector has rotated a nearly integral multiple of half spins to an equivalent position only slightly different from that of the preceding sample. In such cases, it is useful to have N cover an integral number of aliasing periods. We have also found it useful to do an additional smoothing (running average) on the derived values of ϕ and α to reduce any remaining residual modulation caused by a non-uniform sampling of phases.

3c Two Source Effects

We consider the effect of having two sources present with arbitrary strengths, positions, and modulation indices. Let the stronger source A_1 be located at $\phi_1 = 0$ and the weaker source A_2 be located at ϕ_{21}. Let R_T represent the observed sum of the two sources. We have

$$R_1(t) = A_1[1+\alpha_1 \cos 2\omega t]$$
$$R_2(t) = A_2[1+\alpha_2 \cos 2(\omega t-\phi_{21})] \qquad (35)$$
$$R_T(t) = A_T[1+\alpha_T \cos 2(\omega t-\phi_T)]$$

and

$$R_T(t) = R_1(t)+R_2(t) \qquad (36)$$

Then

$$A_T = A_1+A_2$$
$$\alpha_T = \alpha_1\sqrt{[1+2\cos 2\phi_{21}\ A_2\alpha_2/(A_1\alpha_1)+ (A_2\alpha_2)^2/(A_1\alpha_1)^2\ ]}A_1/(A_1+A_2) \qquad (37)$$
$$\tan 2\phi_T = (A_2\alpha_2 \sin 2\phi_{21})/(A_1\alpha_1+A_2\alpha_2 \sin 2\phi_{21}) \qquad (38)$$

Note that ϕ_T, which is the measured shift from source 1 position due to the presence of the weaker source 2, is zero when $\phi_{21} = 90°$, i.e., when the two

sources are at right angles. When $\alpha_2 = 0$ source 2 is isotropic, $\phi_T = 0°$ and

$$\alpha_T = \alpha_1/(1+A_2/A_1) \qquad (38)$$

The behavior of Equation 37 for ϕ_T is plotted in panel A of Figure 3 for a range of source strengths as a function of source separation. Panel B shows the fractional change of modulation index under similar conditions. It is clear that a weak source does not appreciably affect the derived position or modulation index of a strong source.

3f Removal of Modulated Background

In most cases, transient events such as solar bursts or planetary emissions are observed simultaneously with a modulated background component. If the background characteristics (amplitude, direction, modulation index) are relatively constant, then they can be determined before and after the transient event and corrections can be made to obtain the burst characteristics alone.

Let A_0, α_0, and ϕ_0 be the average intensity, modulation index, and position of the background and let A_1, α_1, and ϕ_1 be the measured average intensity, modulation index, and postion of the transient event plus the background. We wish to find A_s, α_s, and ϕ_s characterising the source alone. These quantities are related by

$$A_s[1+\alpha_s\cos 2(\omega t-\phi_s)] = A_1[1+\alpha_1\cos 2(\omega t-\phi_1)-A_0[1+\alpha_0\cos 2(\omega t-\phi_0)] \qquad (40)$$

After simplifying we obtain

$$A_s = A_1-A_0$$
$$\alpha_s = \sqrt{[(\alpha_1A_1)^2-(\alpha_0A_0)^2-2\alpha_1A_1\alpha_0A_0\cos 2(\phi_1-\phi_0)]}/(A_1-A_0) \qquad (41)$$
$$\tan 2\phi_s = [\alpha_1A_1\sin 2\phi_1-\alpha_0A_0\sin 2\phi_0]/[\alpha_1A_1\cos 2\phi_1-\alpha_0A_0\cos 2\phi_0]$$

By standard propagation of error techniques it is possible to derive expressions for the standard deviations of these source determinations in terms of the

standard deviations of the background (0) and the background plus signal (1) parameters. However, the expressions are long and the calculations are best performed during the data processing.

4. APPLICATION TO SIMULATED DATA AND TO REAL DATA

In order to verify the accuracy and features of this processing method, we have found it very useful to generate data with characteristics similar to actual data. For the simulated data we specify the amplitude, position, and modulation index and then see how well the processing method works.

In Section 4a we consider the technique applied to a signal with an abrupt start in the presence of background noise. We show that it is possible to determine the direction of arrival of signals having an intensity only 0.1 that of background. In Section 4b we consider the technique applied to a simulated solar burst. In Sections 4c, 4d, and 4e illustrations are given of spacecraft measurements of real data from solar bursts, Earth emissions, and other planetary emissions.

4a. Simulated Step Signals

In this section we illustrate the results of the processing technique applied to examples of simulated data consisting of a step signal in the presence of background. The input data are computer generated with noise fluctuations having similar statistics to those of data obtained with the Goddard Space Flight Center (GSFC) radio astronomy experiment on IMP-6 (see Brown [1973] for an experiment description). For all examples $\Delta f/f = 0.09$ where Δf is the standard deviation of simulated receiver power with a Gaussian

distribution. A data sampling rate of 11.7 samples per minute and an antenna spin rate of 5.39 rotations per minute are used. These values are similar to those in the IMP-6 experiment and result in observed beat or aliasing periods of 1.05 min (12.3 samples). However, the data-processing technique is not dependent on any particular sampling or spin rate as long as a relatively uniform sampling of phases is used in the processing window. For the cases treated here, the best processing windows contain the closest number of data points to integral multiples of 12.3.

In Figure 4 panel A is a plot of the input data (with no spin) as a function of time. Before t=0, just the background is present. At t=0, a step signal is switched on which is 10 dB above (10 times) background. Panel B of Figure 4 shows these input data with modulation caused by the spacecraft spin. The signal characteristics for this case are signal amplitude =10 dB, modulation index= 0.75, and direction of arrival = 0°. The background characteristics are amplitude= 0 dB and modulation index = 0 (non-directional). Using each 1 minute (12 samples) of signal in panel B as input data $R(t_i)$, the processing technique yields the results plotted in panels C, D, and E. Panel E shows the derived direction of arrival (with a 12 point smoothing) as a function of time. The curve marked "total" is the result of Equation 30 applied to the data in panel B. Prior to time t = 0 min, the derived positions exhibit a random walk as expected for an unmodulated signal. At t = 0 min the computed position shifts towards 0°, which is the true position of the input signal. In panel D, the curve labeled "total" results from Equation 30 applied to the input data. During a ten minute period prior to t = 0, the characteristics (mean intensity, position, and modulation index) were determined for the background using Equations 30; the values obtained were then used in Equations 41 to subtract the background effects. It is seen that for this case a significant correction

towards the true value, $\alpha = 0.75$, occurs, indicating a proper subtraction of background. Panel C is a plot of the derived unmodulated input signal using the values of position and modulation index plotted in panels D and E. Upon comparing panel C to the actual input in panel A, it is seen that the signal restoration is very good, except near $t = 0$, which is at the region of discontinuous change.

In Figure 5, a case is exhibited where the signal is 20 dB above (100 times) background. It is clear that the signal is so large that there is little need for background removal. Figure 6 represents a case with smaller signal intensity now equal to background. Even in this case the true position of 0° is well measured. The modulation index exhibits more scatter because of the lower signal to noise ratio, but, nevertheless, the derived modulation index is an approximation to the input value of 0.75. The errors are similar to those predicted by Equations 34 and and error analysis of Equations 40.

The above simulations were run with a processing window N of 12 data points. To illustrate the power of this signal processing technique for longer processing windows, a value of $n = 123$ points was used in the case shown in Figure 7. In this example the signal amplitude is again equal to the background as in Figure 6, but now is processed with a 10.5 min window. It is evident that a greatly improved determination of the true source position and source modulation index are obtained with this longer window. It is then possible to determine characteristics of even smaller signals. Figure 8 shows a case for the signal intensity only 0.1 that of the background. This input signal is not visible at all in panels A and B. However, the method yields a respectable determination of position (0°) in panel E and modulation index (0.75) in panel D, even for this case where the signal is buried in the noise.

As a final example we show a case where the background is directive and

therefore modulated before and during the time of the signal. For this case, shown in Figure 9, the background characteristics are modulation index = 0.25 and direction of arrival = -60°. The step signal starting at t= 0 has a modulation index = 0.75, direction = 0°, and signal amplitude equal to the background amplitude. It is clear from panels E and D that with background removal, the processing technique yields a very accurate determination of the true signal direction and modulation index.

4b. Simulated Solar Burst

A very common form of sporadic radio event measured by spacecraft experiments is the rapid drift (type III) solar radio burst. We found we can simulate such a burst by a simple function of the form

$$A(t)=t^n \exp(-at) \qquad (42)$$

This function has a maximum $A_{max}= (n/a)^n \exp(-n)$ at time = n/a. If the maximum amplitude is normalized to unity, we have

$$A(t)= (at/n)^n \exp(n-at) \qquad (43)$$

From data obtained from the GSFC experiment on the first Radio Astronomy Explorer satellite (RAE-1) we found that this function simulates the rise and decay of a typical solar burst observed at a frequency near 0.5 MHz for n=4 and a= 1 min where t measures the time from burst start in minutes. Using Equation 43, we proceed with the simulation by introducing computer generated noise and spin modulation with characteristics similar to that used for the step signals in Figures 4 to 9. Figure 10 shows the simulation of a burst 30 dB above a modulated background. Signal and background for a unity gain antenna with no spin are shown in panel A, while panel B shows the observed signal with spacecraft spin. Panels C, D, and E show the output of the processing method

(with a 12 point processing window) using the data in panel B as input. It is clear in panel E how the directions yielded by the processing method switch from a value near -60° to 0° when the burst is present. It is also clear the continuously changing amplitude of the simulated burst does not greatly reduce the accuracy of the position determination, except near the very beginning of the burst where the amplitude change is extremely rapid.

4c. Solar Radio Burst Observations

The first application of the use spacecraft spin modulation to determine the direction of arrival of radio emission was that of Slysh[1967]. By examining the phase of observed spin modulation from data maxima and minima of a short oblique monopole, Slysh made useful determinations of the arrival direction of several solar bursts at 0.2 and 1 MHz. His results were apparently affected by limited information on spacecraft aspect.

The method described in the present paper allows a precise determination to be made of the phase by utilizing all the data points in the spin cycle equally. In Figure 11, we show an example of a real solar burst measured with the GSFC on the IMP-6 spacecraft. The observed modulation is a beat pattern between the sampling rate and the spin rate and is similar in duration to the computer simulations of Figures 4 through 10. Using the real data at 475 kHz in panel A of Figure 11 as input data $R(t_i)$, the processing method outlined in Equations 30 and 32 yield the results shown in panels B,C, and D respectively. The length of the processing window used was N= 12 points. The derived source direction and source modulation index were then smoothed by a 12 point running average before plotting to remove any residual modulation left from a non-uniform sampling of phases. Panel D shows the derived source direction. 0° is the

direction of the Sun, and positive angles are to the west. Before the onset of the burst, the small amount of modulation not readily visible is determined to be coming from the direction of the Earth (77°) as seen from the spacecraft. At the start of the burst the derived direction of arrival quickly shifted to a position about 12° west of the center of the Sun and remained relatively constant for the duration of the burst. Note that the derived direction is not greatly dependent on the burst signal to background ratio as predicted by Equation 37. Panel C is a plot of the derived modulation index. Before the burst, the Earth emission and background have a low level of modulation ($<$ 0.1). The burst itself is almost completely modulated ($\alpha \approx 1$) indicating that this solar burst at this frequency subtends a small angle from IMP-6 and is located very close to spin plane (ecliptic) of the satellite. Panel B is the restored burst amplitude using the values of ϕ and α (plotted in panels A and B) in Equation 32. It is clear that this processing method, applied to actual data, yields results similar to those obtained in the simulation shown in Figure 10.

The utilization of these spin modulated techniques on data obtained over a wide range of frequencies allowed the first tracking of the course of solar radio bursts travelling out from the Sun over distances form 0.1 to 1 AU (Fainberg et al,1972;Fainberg,1973;Fainberg and Stone,1974). In a similar way a movie was prepared showing the centroid of a solar burst progressing out from the Sun along the spiral interplanetary magnetic field in an ecliptic plane projection (Fainberg,1973). A sequence of frames from this movie is shown in Figure 12.

The use of spin modulation to determine arrival direction has also led to the first detection of harmonically related radio emissions (type II) from an interplanetary shock propagating out from the Sun at distances beyond 5 solar

radii (Malitson et al,1973).

4d. Observations of Earth Radio Emissions

It is possible to obtain additional information on the location of radio sources by triangulation from different directions. This technique is particularly effective for satellite observations of radio emissions occurring within the magnetosphere of the Earth. Data from the high sensitivity receivers of the GSFC experiment on IMP-6 indicate that low level radiation is frequently emitted from the Earth at a wide range of frequencies (Stone,1973).

Using the direction of arrival determined form spin modulation, it is possible to accurately track the Earth emissions. Figure 13 shows a projection of an orbit of IMP-6 (1972) in the ecliptic plane. The directions of arrival of radio emission at 130 kHz for selected times are shown as lines from the satellite towards the Earth at angles measured from the spin modulation. They tend to intersect within a small region on the day side of the Earth's projection.

By dividing the 4 day orbit into 3 minute periods, it is possible to form a map of over 3 million possible radio arrival direction intersections. Kaiser and Stone[1975] have reported the results of such a study using triangulation from orbits extending over 500 days of observations in which 2 sources are evident. Figure 14 is a summary of their findings at 130 kHz. The source on the day side is lower in intensity but is present more often than the second (nightside) source which is very sporadic and intense.

4e. Detection of Other Planetary Emissions

By examining the IMP-6 observations for periods when the measured source locations were in the direction of Jupiter, Brown [1974] was able to make the first detection of Jupiter radio emission at low frequencies. An example of the measured direction of arrival of a Jupiter radio burst is shown in Figure 15. Prior to the burst which started near 0900 on April 25,1972, the measured direction of arrival of the radio emission was west of the direction of the Earth. At the start of the burst, the measured position quickly shifted towards the direction of Jupiter, where it stayed for the duration of the burst. In this manner, Brown was able to locate, identify, and study a large number of Jupiter bursts within the frequency range of 425- 9900 kHz in 1971 and 1972.

Using similar direction finding techniques with the IMP-6 data, Brown [1975] was able to make the first detection and measurement of nonthermal radio emissions from the planet Saturn. The spectral analysis of these bursts may yield valuable information on the planet's radiation belts and magnetic field strength.

5. SUMMARY AND FUTURE WORK

The data processing technique described in this paper has allowed a very accurate and fast determination to be made of source direction and characteristics using spin modulation of the IMP-6 GSFC radio data. This permitted radio techniques to be used to detect and study processes occuring at long distances from the observing spacecraft. In the case of solar emission, it has provided the first radio visualization of the curvature of the interplanetary magnetic field caused by solar rotation. If several spinning spacecraft separated by

large distances observe the same event, source location via triangulation from extended baselines is possible, independent of models of emission levels. Such observations (eg between HELIOS and ISEE 3) will also yield valuable information on gross magnetic field structure and plasma density along the trajectories of the particles responsible for the burst.

In the case of emissions from Earth and other planets, it is clear that the radio techniques will permit the exploration via remote sensing of many particle-field interactions occurring in the planetary magnetospheres.

Several extensions of these techniques are possible. For sporadic events where the amplitude changes are more rapid, it is possible to derive better information on source direction and modulation index by allowing for this. A method involving least squares fitting has been derived and utilized on IMP-6 data and will be described in a future report. The least squares technique also allows a better way of weighting the data which leads to increased accuracies.

A very important enhancement of the spin modulation technique is possible if the spinning dipole is located out of the spin plane (as it was for Slysh [1967]). For that case the spin modulation signal R(t) from a distant source for an antenna short compared to wavelength is of the form

$$R(t)= [1+ a_1 \cos(\omega t-\omega t_0-\phi) + a_2 \cos 2(\omega t-\omega t_0-\phi)]A \qquad (44)$$

where A is a measure of the source strenth, ϕ is the source direction projected into the spin plane, and a_1 and a_2 are quantities which permit the determination of the other angle describing the center of the source direction (elevation angle out of the spin plane). In the case of a uniformly distributed source this technique yields both angles describing the centroid of the source, as well as the half-width of the source, thus removing the ambiguity illustrated in Figure 2.

A satellite experiment (Knoll et al,1978) based on this latter technique of

an oblique spinning dipole (electrically formed) has been developed and is included on the International Sun Earth Explorer (ISEE 3, launched in August 1978) as a joint experiment of the Meudon (France) and GSFC (USA) radio astronomy groups.

Acknowledgement

I acknowledge with much gratitude the encouragement and advice I received during the active phase of this work from the GSFC IMP-6 radio astronomy team, particularly R.G. Stone, M.L. Kaiser, H.H. Malitson, L.W. Brown, R.R. Weber, J. Alexander, and S. Kayser.

APPENDIX A : ERROR ANALYSIS

In this appendix expresions are derived for the errors in the determination of the direction of arrival and the modulation index in the presence of an unmodulated background.

1. General Gain Function

Using the notation as in Section 2, where $R(t_i)$= observed signal at time t_i, $G(\phi)$= normalized gain in direction ϕ, $A(t_i)$= signal observed by unity gain and $B(t_i)$= background measured at time t_i, we have

$$R(t_i)= G(\phi-\omega t_i)A(t_i) + B(t_i) \tag{45}$$

Expanding G in a Fourier series we have

$$G(\phi)= \Sigma\, b_j \cos j\phi + a_j \sin j\phi \tag{46}$$

or equivalently

$$G(\phi)= \Sigma\, d_j \cos j(\phi-e_j) \tag{47}$$

Assume that the signal ampltude A(t) does not change significantly within the processing window of N points and that the mean value of $A(t_i)$ over the processing window is A. We define the quantities C_k, S_k, and C_0

$$\begin{aligned} C_k &= \Sigma\, R(t_i)\cos k\omega t_i \\ S_k &= \Sigma\, R(t_i)\sin k\omega t_i \\ C_0 &= \Sigma\, R(t_i) \end{aligned} \tag{48}$$

Since N is a value such that phases of the trigonometric functions appear uniform in the sums, we have by standard Fourier techniques the following expressions for the mean values

$$\begin{aligned} C_k &= \frac{N}{2} Ab_k \cos k\phi_s + \frac{N}{2} Aa_k \sin k\phi_s \\ S_k &= \frac{N}{2} Ab_k \sin k\phi_s - \frac{N}{2} Aa_k \cos k\phi_s \\ C_0 &= NAb_0 + NBb_0 \end{aligned} \tag{49}$$

It can be shown that these Equations result from a least squares fitting of Equation 45 to the data measured in the processing window. We are interested in the variances of C_k, S_k, and C_0, and write these quantities as var C_k, var S_k, and var C_0 respectively. We have

$$\text{var } C_k = \text{var } [\sum_i \sum_j d_j \cos j(\phi_s - \omega t_i - e_j) A(t_i) \cos k\omega t_i + \sum_i B(t_i) \cos k\omega t_i] \quad (50)$$

Interchanging the i and the j summations

$$\text{var } C_k = \text{var } [\sum_j d_j \sum_i x_i + \sum_i y_i \quad (51)$$

where

$$x_i = \cos j(\phi_s - \omega t_i - e_j)\ A(t_i)\ \cos k\omega t_i$$

$$y_i = B(t_i)\ \cos k\omega t_i$$

Since x_i and y_i are statistically independent

$$\text{var } C_k = \sum_j d_j^2 \sum_i \text{var } x_i + \sum_i \text{var } y_i \quad (52)$$

Let $\theta = \omega t_i$ and let $\text{var}_\theta\ x_i$ be the contribution to var x_i for a particular value of θ. Then

$$\text{var}_\theta\ x_i = \cos^2 j(\phi_s - \theta - e_j)\ \cos^2 k\theta\ \text{var } A(t_i) \quad (57)$$

Since all θ (modulo 2π) are equally probable

$$p(\theta)\, d\theta = d\theta/2\pi \quad (54)$$

where p is the probability of θ being between θ and $\theta + d\theta$. Then

$$\text{var } x_i = \int p(\theta)\ \text{var}_\theta\ x_i\ d\theta \quad (55)$$

Using Equations 57 and 55 for $k \neq 0$

$$\begin{aligned} \text{var } x_i &= \tfrac{1}{2} \text{ var } A && \text{for } j = 0 \\ &= \tfrac{1}{4} \text{ var } A && \text{for } j \neq k \\ &= \tfrac{1}{4} [\ 1 + \tfrac{1}{2} \cos 2k(\phi_s - e_k)\ ] \text{ var } A && \text{for } j = k \neq 0 \quad (56) \end{aligned}$$

$$\text{var } y_i = \tfrac{1}{2} \text{ var } B$$

where var A, var B are the variances of $A(t_i)$ and $B(t_i)$ respectively. Using Equations 56 and 57

$$\text{var } C_k = \frac{N}{2}\left[d_0^2 + \frac{1}{2}\sum_j d_j^2 + \frac{1}{4} d_k^2 \cos 2k(\phi_s - e_k) \right] \text{var } A + \frac{N}{2} \text{var } B \qquad (57)$$

$$\text{var } S_k = \frac{N}{2}\left[d_0^2 + \frac{1}{2}\sum_j d_j^2 - \frac{1}{4} d_k^2 \cos 2k(\phi_s - e_k) \right] \text{var } A + \frac{N}{2} \text{var } B \qquad (58)$$

$$\text{var } C_0 = \frac{N}{2}\left[2d_0^2 + \sum_j d_j^2 \right] \text{var } A + \text{var } B \qquad (59)$$

We obtain the standard deviations

$$\Delta C_k = \sqrt{(\text{var } C_k)}$$
$$\Delta S_k = \sqrt{(\text{var } S_k)} \qquad (60)$$
$$\Delta C_0 = \sqrt{(\text{var } C_0)}$$

Note that $\Delta C_k / C_k \sim \Delta A/(A\sqrt{N}) \ll 1$ for large signal to background values. This applies also to ΔS_k and ΔC_0.

2. Dipole Gain Function

For a dipole antenna with length short compared to wavelength measuring a source with modulation index α we have for the normalized gain function

$$G(\phi) = (1+\alpha\cos 2\phi)/(1+\alpha) \qquad (61)$$

From Equations 49

$$C_2 = \tfrac{1}{2}[NA\alpha\cos 2\phi_s)]/(1+\alpha)$$
$$S_2 = \tfrac{1}{2}[NA\alpha\sin 2\phi_s)]/(1+\alpha)$$
$$C_0 = (NA+NB)/(1+\alpha)$$

From Equations 60

$$\Delta C_2 = \sqrt{\left[1 + \frac{1}{2}\alpha^2 + \frac{1}{4}\alpha^4 \cos 4\phi_s + (1+\alpha)^2 \Delta B^2/\Delta A^2 \right]} \Delta A \sqrt{N}/[(1+\alpha)\sqrt{2}]$$
$$\Delta S_2 = \sqrt{\left[1 + \frac{1}{2}\alpha^2 - \frac{1}{4}\alpha^4 \cos 4\phi_s + (1+\alpha)^2 \Delta B^2/\Delta A^2 \right]} \Delta A \sqrt{N}/[(1+\alpha)\sqrt{2}] \qquad (63)$$
$$\Delta C_0 = \sqrt{\left[1 + \frac{1}{2}\alpha^2 + (1+\alpha)^2 \Delta B^2/\Delta A^2 \right]} \Delta A \sqrt{N}/(1+\alpha)$$

To calculate the rms error $\Delta\phi_s$ use

$$\tan 2\phi_s = S_2/C_2 \qquad (64)$$

Then

$$\Delta\phi_s = \sqrt{[\ 1 + \tfrac{1}{4}\alpha^2 + (1+\alpha)^2\ \Delta B^2/\Delta A^2\ ]}\ \Delta A/[\alpha\sqrt{(2N)}]$$

In a similar way we find the error in α (for large signal to noise case)

$$\Delta\alpha = \sqrt{[2-3\alpha^2/2+\alpha^4/2]}\ \Delta A/(A\sqrt{N}) \qquad (65)$$

APPENDIX B - OBSERVED SIGNAL

In this appendix we derive the expression for a signal observed by a short dipole antenna with a gain function $G(\phi) = \frac{1}{2} + \frac{1}{2}\cos\phi$. Section B1 deals with a point source located at an angle θ from the spin axis. Section B2 deals with a uniform source.

B1. Point Source

Let $\underline{s}$ be the unit vector pointing toward a point source so that

$$\underline{s} = (\sin\theta_s\cos\phi_s,\ \sin\theta_s\sin\phi_s,\ \cos\theta_s) \qquad (67)$$

Where θ_s and ϕ_s are the polar and azimuthal angles. Let $\underline{a}$ be the unit vector in the spin (azimuth) plane along the dipole axis. Then

$$\underline{a} = (\cos(\omega t + \pi/2),\ \sin(\omega t + \pi/2), 0) \qquad (68)$$

where ωt is the azimuthal angle to the dipole normal in the spin plane. The response of the short dipole to the source with strength A(t) is given by

$$R(t) = [\ 1-(\underline{a}\cdot\underline{s})^2\ ]\ A(t) \qquad (69)$$

After substitution

$$R(t) = [\ 1+\alpha\cos2(\omega t-\phi_s)\ ]\ \frac{1}{\alpha}\ A(t) \qquad (70)$$

where α is given by

$$\alpha = \sin^2\theta_s/(2-\sin^2\theta_s) \qquad (71)$$

2. Uniform Conical Source

We consider a source having a uniform intensity over a cone with half angle γ and axis located in the y-z plane at an angle β from the dipole axis (z-axis). If $d\Omega$ is a small solid angle within the conical source located at an angle θ from the dipole axis, its contribution to the total signal R is

$$dR = A\sin^2\theta d\Omega \tag{72}$$

where A is a measure of the source strength. Then

$$R = A \int_{\text{source}} \sin^2\theta d\Omega \tag{73}$$

Initially we place the dipole along the z-axis so that

$$R = A \int_{\text{source}} (1-z^2)\, d\Omega \tag{74}$$

where z is the component of the unit vector towards $d\Omega$. To evaluate this integral over the source, we first rotate coordinates through an angle β about the x-axis to a primed set of coordinates such that the negative z-axis is along the cone axis. Then

$$z = z'\cos\beta - y'\sin\beta \tag{75}$$

and

$$z^2 = z'^2\cos^2\beta + y'^2\sin^2\beta - 2y'z'\sin\beta\cos\beta \tag{76}$$

Let θ', ϕ' be polar cooordinates with respect to the z'-axis. Then

$$\begin{aligned} y' &= \sin\theta'\cos\phi' \\ z' &= \cos\theta' \\ d\Omega &= \sin\theta d\theta d\phi = \sin\theta' d\theta d\phi \end{aligned} \tag{77}$$

In the primed coordinates, Equation (74) becomes

$$R = A\int_0^{2\pi} d\phi' \int_0^{\gamma} d\theta' \sin\theta'[1-z'^2\cos^2\beta - y'^2\sin^2\beta + 2y'z'\sin\beta\cos\beta] \tag{78}$$

After substituting Equations (77) we find after integrations that

$$R = 2\pi A(B - C\cos^2\beta) \tag{79}$$

where

$$B = \frac{2}{3} - \frac{1}{2}\cos\gamma - \frac{1}{6}\cos^3\gamma$$

$$C = \frac{1}{2}\cos\gamma\sin^2\gamma$$

Equation 79 yields the response of a dipole inclined at an angle β to the cone axis. We consider a new xyz coordinate system where the cone axis is the unit vector $\underline{c}$ and is inclined at an angle θ_c to the z-axis with azimuthal angle ϕ_c in the xy plane. We let the dipole unit vector $\underline{a}$ be in the xy plane and measure the azimuthal angle to its normal from the x-axis. Then

$$\underline{a} = (\cos[\omega t+\pi/2], \sin[\omega t+\pi/2], 0) \tag{80}$$

$$\underline{c} = (\sin\theta_c\cos\phi_c, \sin\theta_c\sin\phi_c, \cos\theta_c) \tag{81}$$

$$\cos^2\beta = (\underline{a}\cdot\underline{c})^2 \tag{82}$$

and finally

$$\cos^2\beta = \sin^2\theta_c[1-\cos2(\omega t-\phi_c)]/2 \tag{83}$$

After inserting in Equation 79 we find

$$R(t) = [1+\alpha\cos2(\omega t-\phi_c)]A'(t) \tag{84}$$

where

$$\alpha = \sin^2\theta_c/(2B/C - \sin^2\theta_c) \tag{85}$$

and $A'(t)$ is a measure of the source strength. Note that for small cone widths γ, Equation 85 reduces to Equation 71.

REFERENCES

Brown,L.W.(1973),The galactic radio spectrum between 130 and 2600 kHz,Astophys. J.180,359-370

Brown,L.W.(1974a),Jupiter emission observed near 1 MHz,Astrophys.J.192,547-550

Brown,L.W.(1974b),Spectral behavior of Jupiter near 1 MHz,Astrophys.J.Lett.194, L159-L162

Brown,L.W.(1975),Saturn radio emission near 1 MHz,Astrophys.J.Lett.198,L89-L92

Fainberg,J.,L.G.Evans,and R.G.Stone(1972),Radio tracking of energetic particles through interplanetary space,Science 178,743-745

Fainberg,J.(1973),Solar radio bursts ot low frequencies,IAU Symp. 57 on Coronal Disturbances, Surfer's Paradise,Australia,Coronal Disturbances, 183-200,G.Newkirk,Jr.(ed.),D.Reidel Pub.Co.,Dordrecht,Netherlands,

Fainberg,J.and R.G.Stone(1974),Satellite observations of type III solar radio bursts at low frequencies,Sp.Sci.Rev.16,145-188

Jackson,J.P.(1962),Classical Electrodynamics,278,John Wiley & Sons, New York

Kaiser,M.L.,and R.G.Stone(1974),Earth as an intense planetatry radio source: similarities to Jupiter and Saturn, Science 189,285-287

Kraus,J.D.(1966),Radio Astronomy,244,McGraw-Hill,New York

Knoll,R.,G.Epstein,S.Hoang,G.Huntzinger,J.L.Steinberg,J.Fainberg,F.Grena, S.R.Mosier,and R.G.Stone(1978),The 3-dimensional radio mapping experiment (SBH) on ISEE-C,IEEE Trans.Geoscience Electr.GE-16,No 3,199-204

Lecacheux,A.,C.C.Harvey,and A.Boishot(1979),Source localisation and polarisation determination in low frequency radio astronomy,Annales des Télécom.35 (3-4),254-265

Malitson,H.H.,J.Fainberg,and R.G.Stone(1973),Observation of a type II solar radio burst to 37_o,Astrophys.Lett.14,111-114

Slysh,V.I.(1967),Observation of long wavelength solar radio emission by the spacecraft Luna XI and Luna XII,Kosm.Issled.5,897-910,(trans. Cosmic Res.5,759-769)

Steinberg,J.L.(1979),Satellite observations of solar radio bursts,IAU Symp. No.86,Radio Physics of the Sun, Univ. of Maryland

Stone,R.G.(1973),Radio physics of the outer solar system,Space Sci.Rev.14, 534-551

FIGURE CAPTIONS

FIGURE 1. Dipole gain coefficients for the first four terms in the Fourier expansion for a range of normalized antenna lengths. For $D/\lambda < 0.5$, only the first two terms are significant.

FIGURE 2. Modulation index for a circular conical source with uniform intesity as a function of the source width and elevation angle of the source center above the spin plane. For example, a modulation index of 0.2 can result from a narrow source located at an elevation angle near 55° above (or below) the spin plane. Wider sources must be located at lower elevation angles.

FIGURE 3. Two source effects. A) If a second source is present, the direction of arrival measured for the combination departs from the direction of source 1 by the amount shown. If the second source can be measured alone, then a correction can be made analytically. B) If a second source is present with modulation index the same as source 1, then the combined modulation index measured departs from that of source 1 by the amount shown. If the second source can be measured alone, then a correction can be made analytically.

FIGURE 4. Application of the processing method to computer simulated data with receiver noise and sampling characteristics similar to those of the GSFC experiment on IMP-6. Panel A shows the generated data without spin. Panel B shows the generated modulated data with an unmodulated background present at all times. At t= 0 min a 10 dB step is switched on with a modulation index of 0.75 and with a direction of arrival of 0°. Panels C, D, and E show results obtained from the processing method applied to input data from panel B with a processing window of

12 successive points (1 min of data). For the curve marked "background removed" the background characteristics were determined by the processing method using 10 min of data prior to the signal step, and were removed using Equation 41.

FIGURE 5. Same as figure 4, but with a signal amplitude 20 dB above background. Background removal is seen not to be necessary for large signal to background values.

FIGURE 6. Same as figure 4, but with a signal amplitude equal to the background. Panel D shows the correction provided by the background removal techniques (Equations 41).

FIGURE 7. Same as figure 6, but with a processing window 10 times as long. Note the improved derived direction of arrival (panel E) and derived modulation index (panel D) for this example with a processing window of 123 points (10.5 min of data).

FIGURE 8. Same as figure 7, but with a signal step only 0.1 times background. The input signal is not visible in panel B but, nevertheless, the processing method does yield a determination of the arrival direction and modulation index. This shows the power of the data processing technique for longer processing windows (123 points or 10.5 min of data).

FIGURE 9. In this case the background is also modulated with a direction of -60° and modulation index 0.25. The signal size is equal to the background in amplitude but has an arrival direction of 0° and a modulation index of 0.75. The background characteristics are measured during a 10 min section of data before the step and are used in panels D and E for background removal using Equations 41.

FIGURE 10. Computer generated data simulating the rise and decay of a solar

burst. The background is modulated with an arrival direction of -60° and modulation index 0.75. Panels D and E show the measured characteristics to be similar to the burst during the period when the burst amplitude is above the background level.

FIGURE 11. Actual data from IMP-6 observations of a solar burst measured of 23 June 1971 are plotted in panel A. Panels B,C,and D, show the results of the processing method applied to the data in panel A. The derived direction of arrival before the solar burst is determined to be from the direction of the Earth (77°). At the start of the burst the direction quickly shifts to a location 12° west of the center of the Sun (0°).

FIGURE 12. Frames from a movie showing the evolution of the centroid of a solar burst as determined from the measured arrival direction and amplitudes, using IMP-6 data. Each frame is a collection of two minutes of data plotted in an ecliptic plane projection with the Sun at the center, and the Earth and the IMP-6 satellite at the bottom at 0°. Circles located at increments of 50 solar radii from the Sun are drawn. Emission at different radio frequencies originates at different emission levels in the outer corona of the Sun. The locations of plotted radial line segments (with length proportional to signal amplitude) are determined from the intersections of the measured directions of arrival with average spherical coronal emission levels. The centroid of a travelling solar radio burst caused by energetic particles moving out from the Sun along the spiral interplanetary magnetic field is shown evolving in the successive 2-minute frames (after Fainberg,1974).

FIGURE 13. Outline of orbit 74 in 1972 of IMP-6 spacecraft; shown are measured

arrival directions of radio noise at 130 kHz during selected times projected in the ecliptic plane. These directions intersect in a small region on the day side of the Earth.

FIGURE 14. Occurence rates of intersections of arrival directions at 130 kHz similar to those shown in figure 13. These data summarize 500 days of IMP-6 observations (for discussion, see Kaiser and Stone[1975]).

FIGURE 15. Detection of radio burst coming from Jupiter observed with IMP-6. 0° on the angle plot is the direction of the Sun. Positive angles are to the west. Prior to 0900, the direction of arrival of the radiation quickly shifted towards Jupiter. In this way, the first detection of emission from Jupiter at low frequencies was made (Brown,1974). At this time the beat period between the sampling rate and spin rate was much shorter than in figure 11 and is not visible as a spin modulation pattern. A processing window of 32 points (2.5 min) was used.

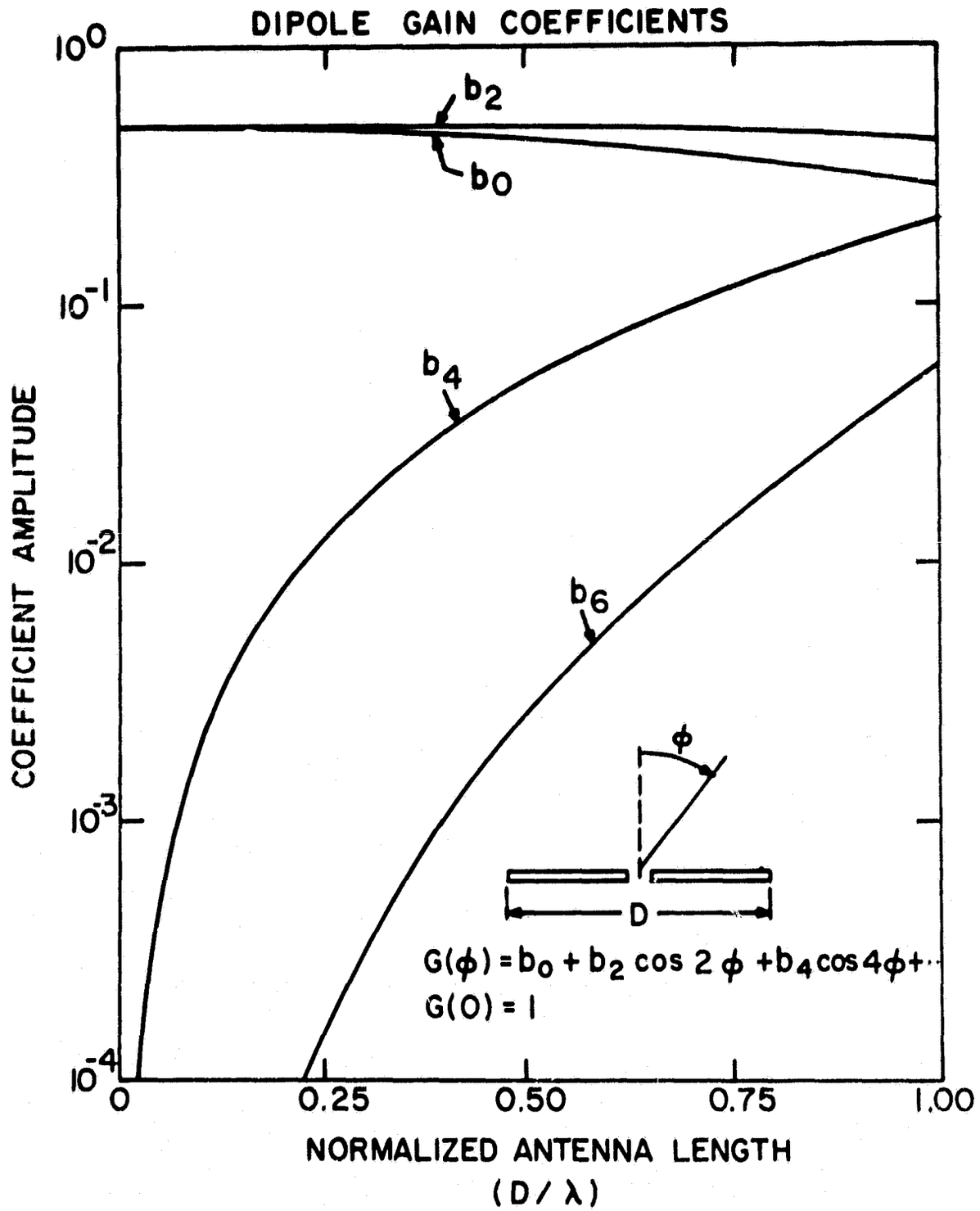
DIPOLE GAIN COEFFICIENTS
10^0
10^{-1}
10^{-2}
10^{-3}
10^{-4}
b_2
b_0
b_4
b_6
COEFFICIENT AMPLITUDE
ϕ
D
$G(\phi) = b_0 + b_2 \cos 2\phi + b_4 \cos 4\phi + \cdots$
$G(0) = 1$
0
0.25
0.50
0.75
1.00
NORMALIZED ANTENNA LENGTH
(D/λ)

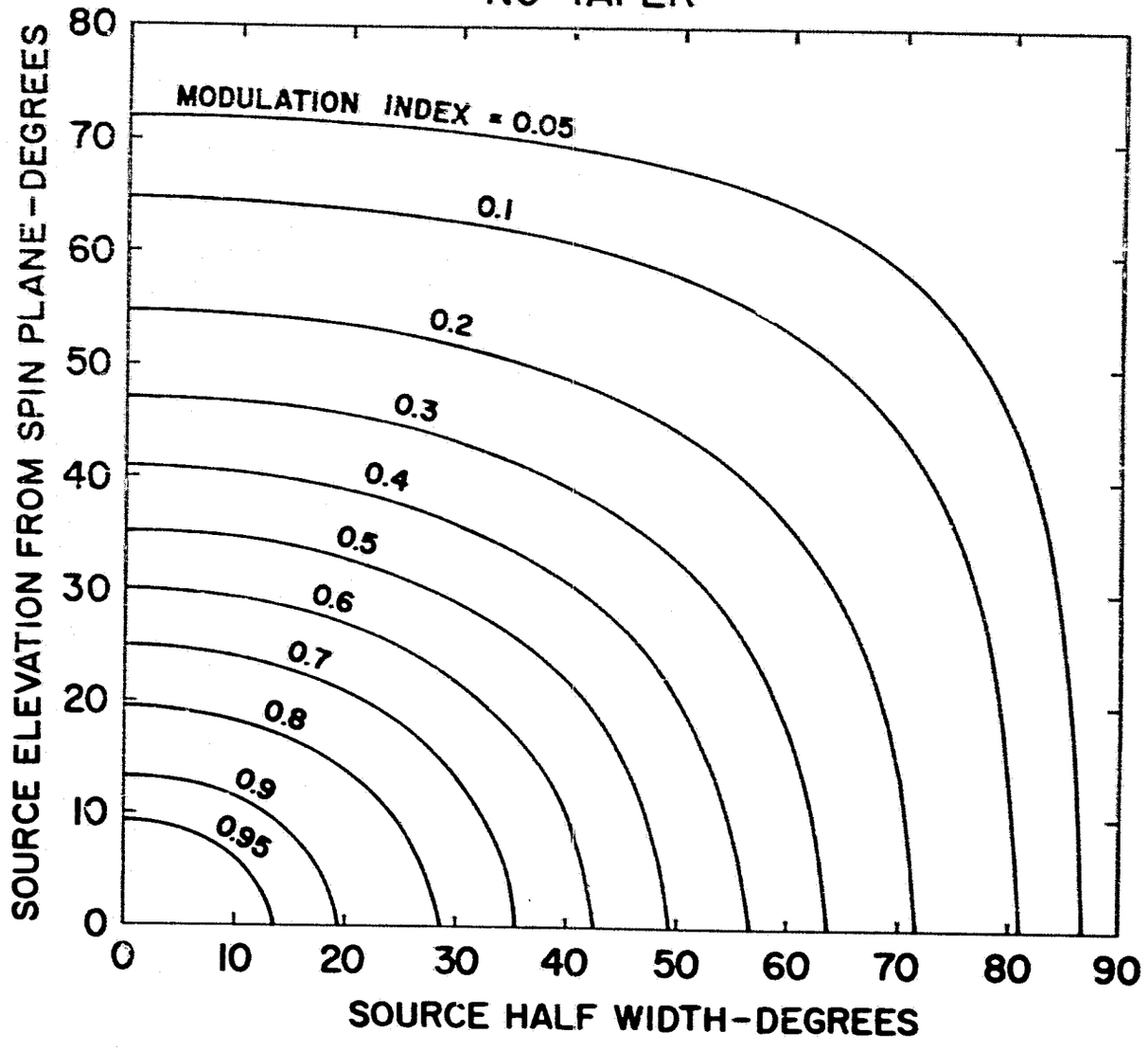
CIRCULAR SOURCE
NO TAPER
MODULATION INDEX = 0.05
0.1
0.2
0.3
0.4
0.5
0.6
0.7
0.8
0.9
0.95
SOURCE ELEVATION FROM SPIN PLANE-DEGREES
SOURCE HALF WIDTH-DEGREES
0
10
20
30
40
50
60
70
80
90

A

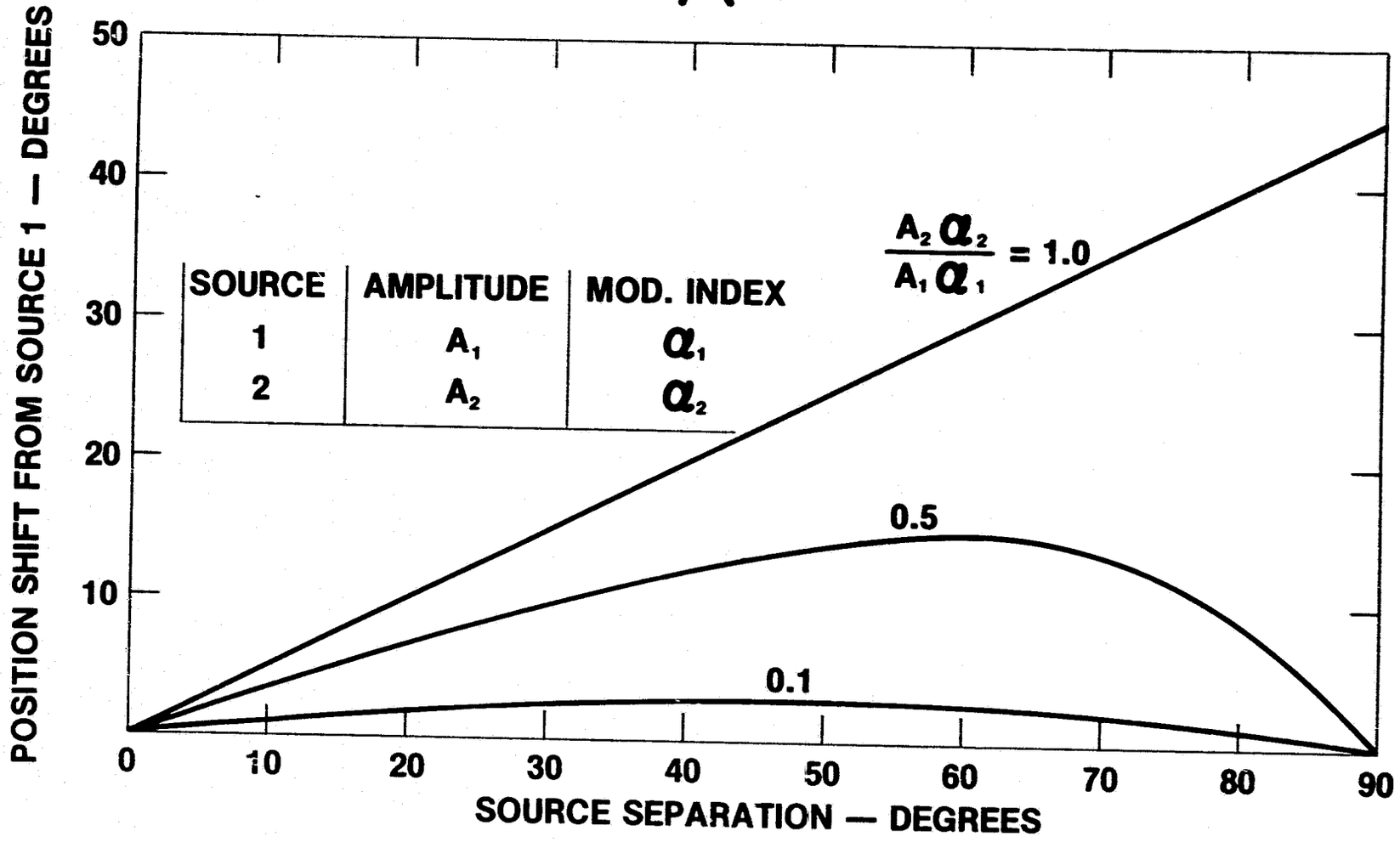
POSITION SHIFT FROM SOURCE 1 — DEGREES
50
40
30
20
10
0
10
20
30
40
50
60
70
80
90
SOURCE SEPARATION — DEGREES
SOURCE | AMPLITUDE | MOD. INDEX
1 | A1 | α1
2 | A2 | α2
A2 α2 / A1 α1 = 1.0
0.5
0.1

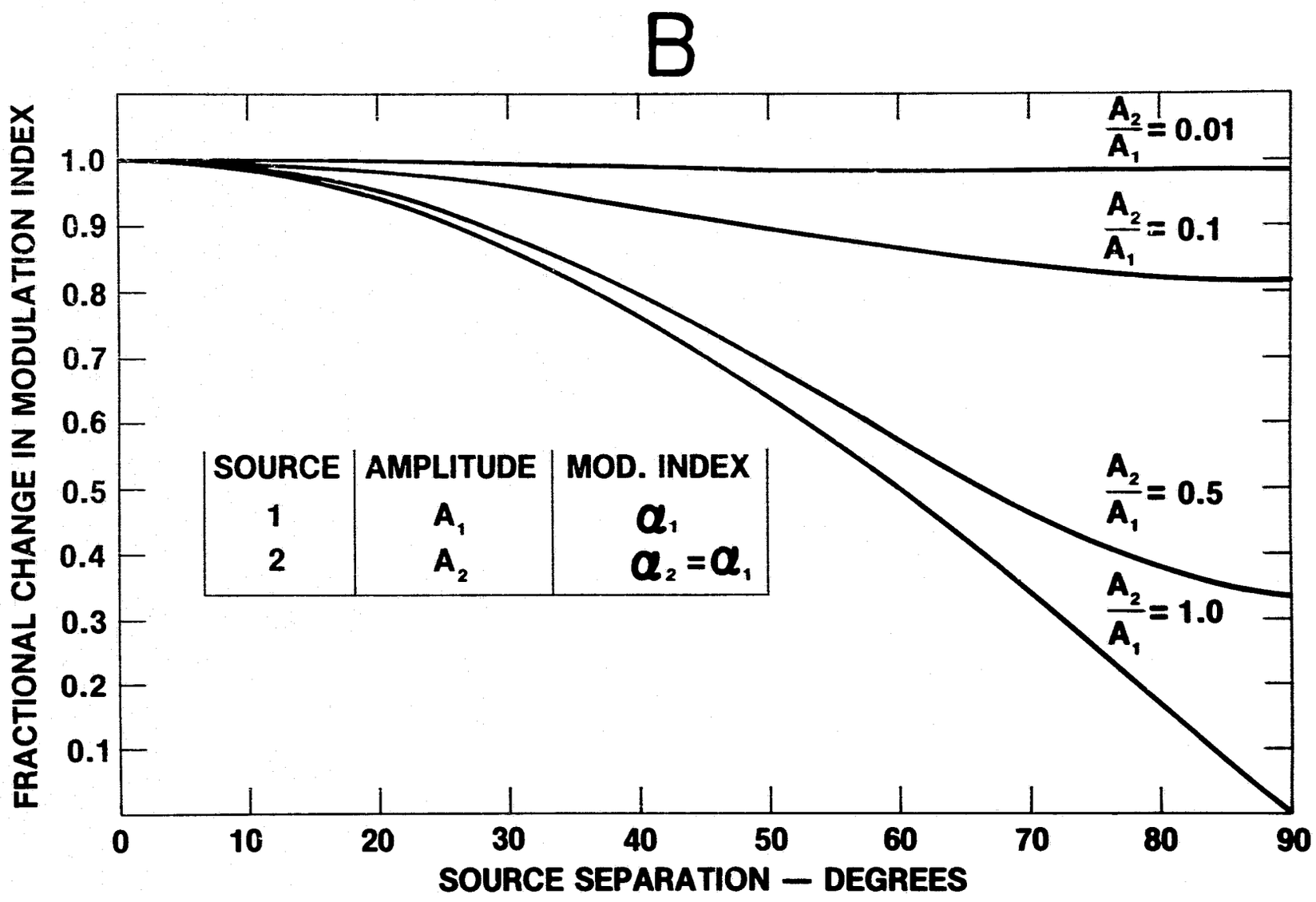
B
FRACTIONAL CHANGE IN MODULATION INDEX
1.0
0.9
0.8
0.7
0.6
0.5
0.4
0.3
0.2
0.1
0
10
20
30
40
50
60
70
80
90
SOURCE SEPARATION — DEGREES
A2/A1 = 0.01
A2/A1 = 0.1
A2/A1 = 0.5
A2/A1 = 1.0
SOURCE | AMPLITUDE | MOD. INDEX
1 | A1 | α1
2 | A2 | α2 = α1

FIGURE 3B

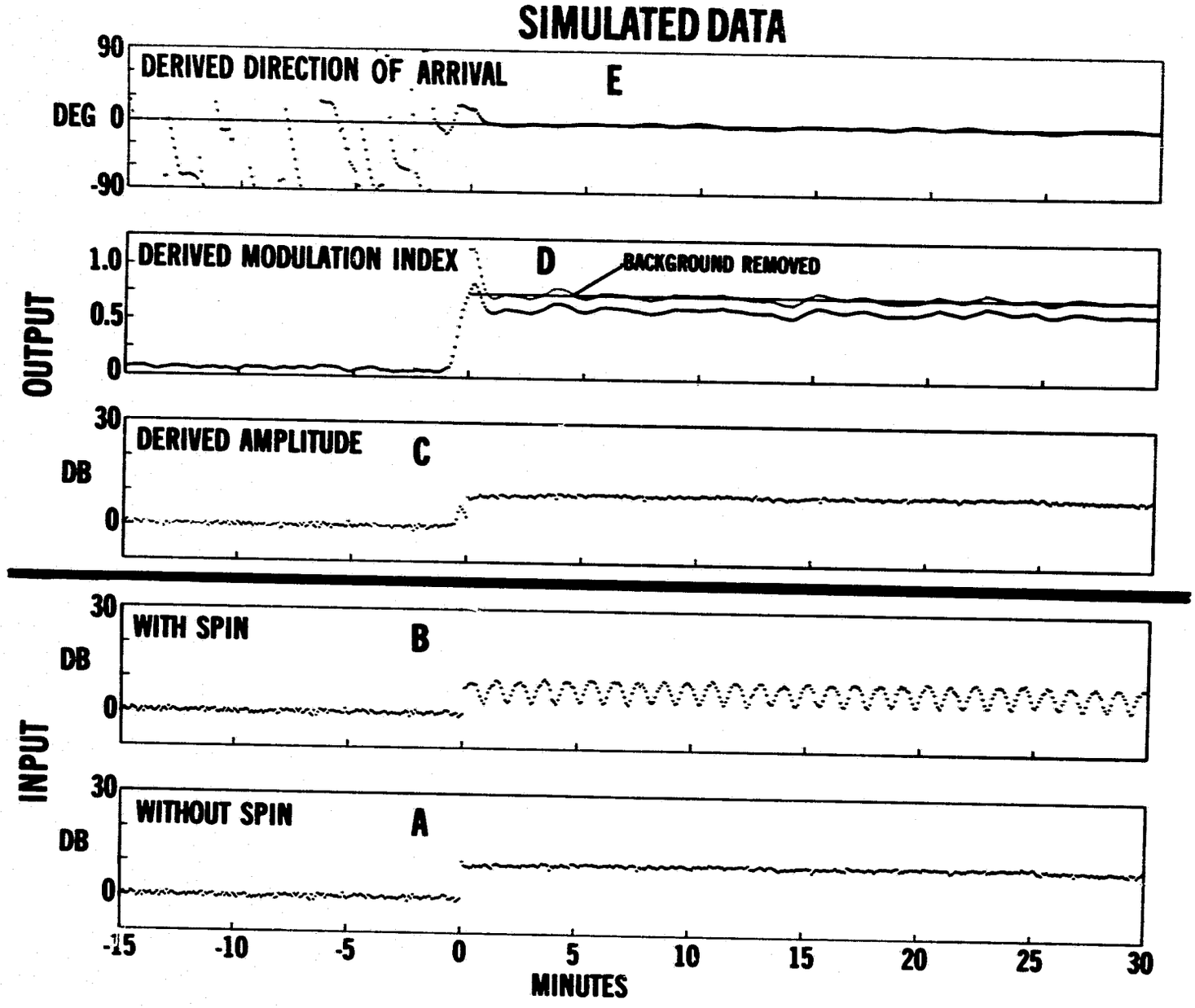
SIMULATED DATA
90
DERIVED DIRECTION OF ARRIVAL
E
DEG 0
-90
1.0
DERIVED MODULATION INDEX
D
BACKGROUND REMOVED
0.5
OUTPUT
0
30
DERIVED AMPLITUDE
C
DB
0
30
WITH SPIN
B
DB
0
INPUT
30
WITHOUT SPIN
A
DB
0
-15
-10
-5
0
5
10
15
20
25
30
MINUTES

FIGURE 4

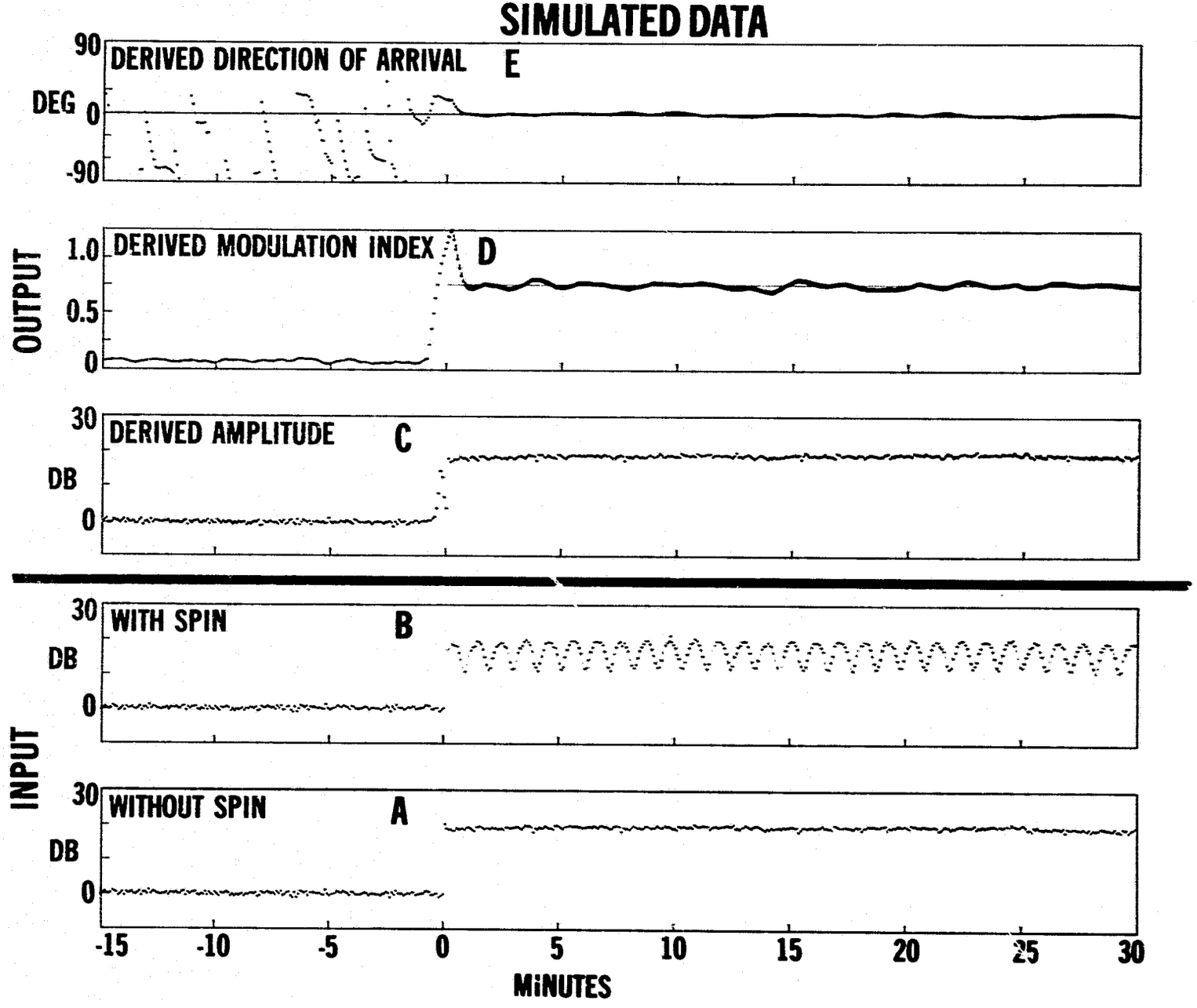
SIMULATED DATA
90
DERIVED DIRECTION OF ARRIVAL
E
DEG
0
-90
OUTPUT
1.0
DERIVED MODULATION INDEX
D
0.5
0
30
DERIVED AMPLITUDE
C
DB
0
INPUT
30
WITH SPIN
B
DB
0
30
WITHOUT SPIN
A
DB
0
-15
-10
-5
0
5
10
15
20
25
30
MINUTES

FIGURE 5

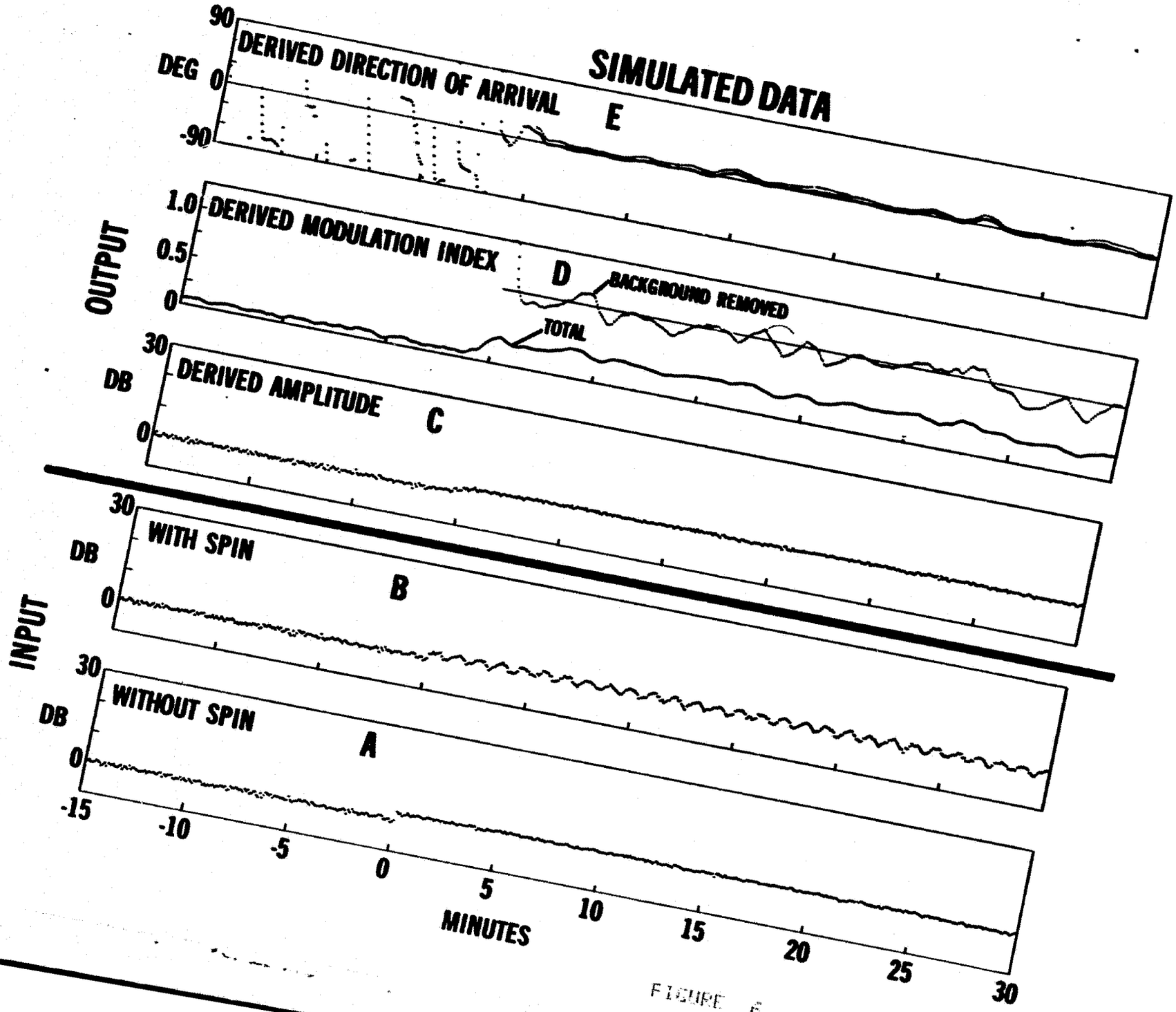
SIMULATED DATA
90
DEG 0
-90
DERIVED DIRECTION OF ARRIVAL
E
1.0
0.5
0
OUTPUT
DERIVED MODULATION INDEX
D
BACKGROUND REMOVED
TOTAL
30
DB
0
DERIVED AMPLITUDE
C
30
DB
0
WITH SPIN
B
INPUT
30
DB
0
WITHOUT SPIN
A
-15
-10
-5
0
5
10
15
20
25
30
MINUTES

FIGURE 6

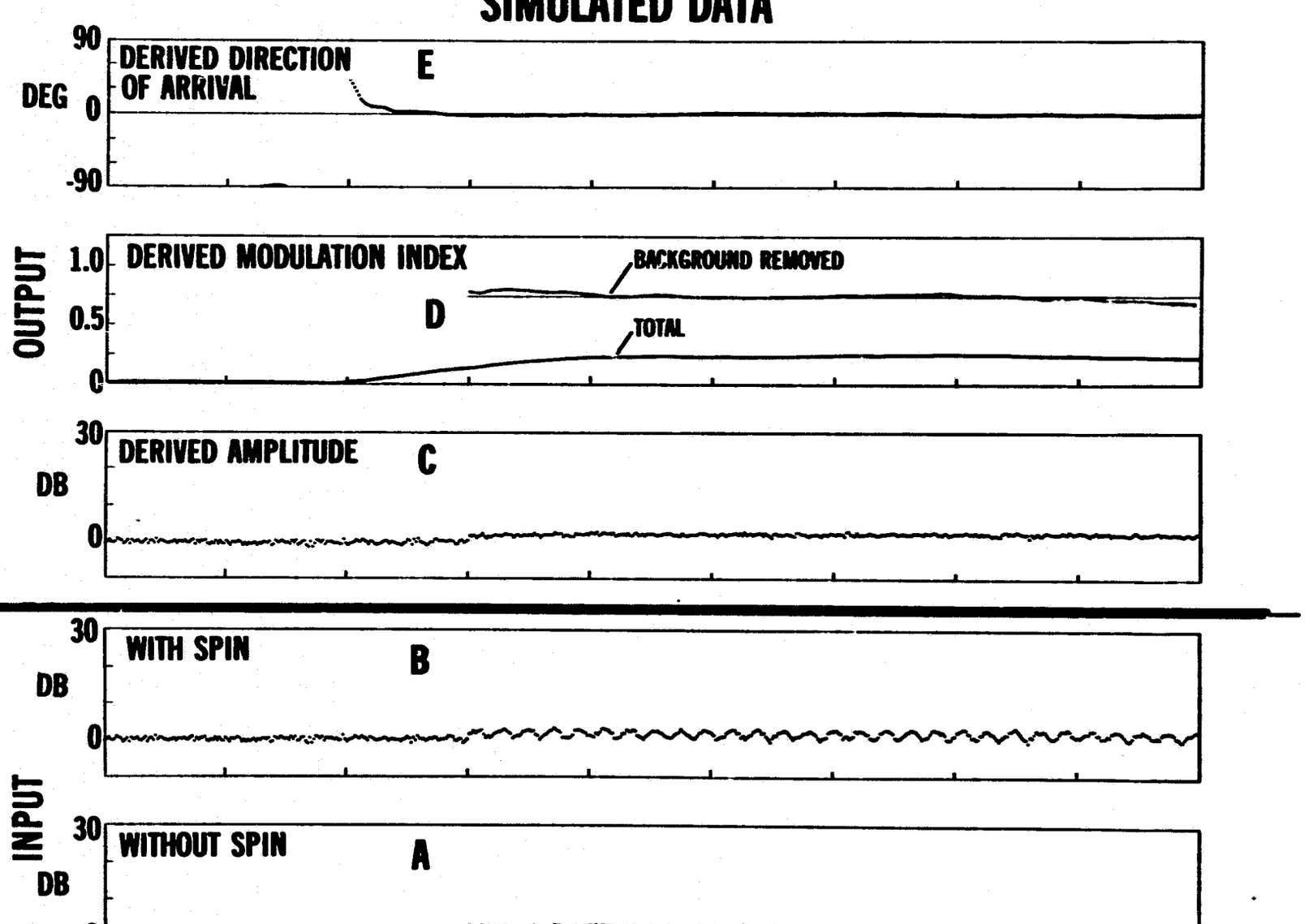
SIMULATED DATA
90
DEG
0
-90
DERIVED DIRECTION OF ARRIVAL
E
OUTPUT
1.0
0.5
0
DERIVED MODULATION INDEX
BACKGROUND REMOVED
D
TOTAL
30
DB
0
DERIVED AMPLITUDE
C
30
DB
0
WITH SPIN
B
INPUT
30
DB
0
WITHOUT SPIN
A
-15
-10
-5
0
5
10
15
20
25
30
MINUTES

FIGURE 7

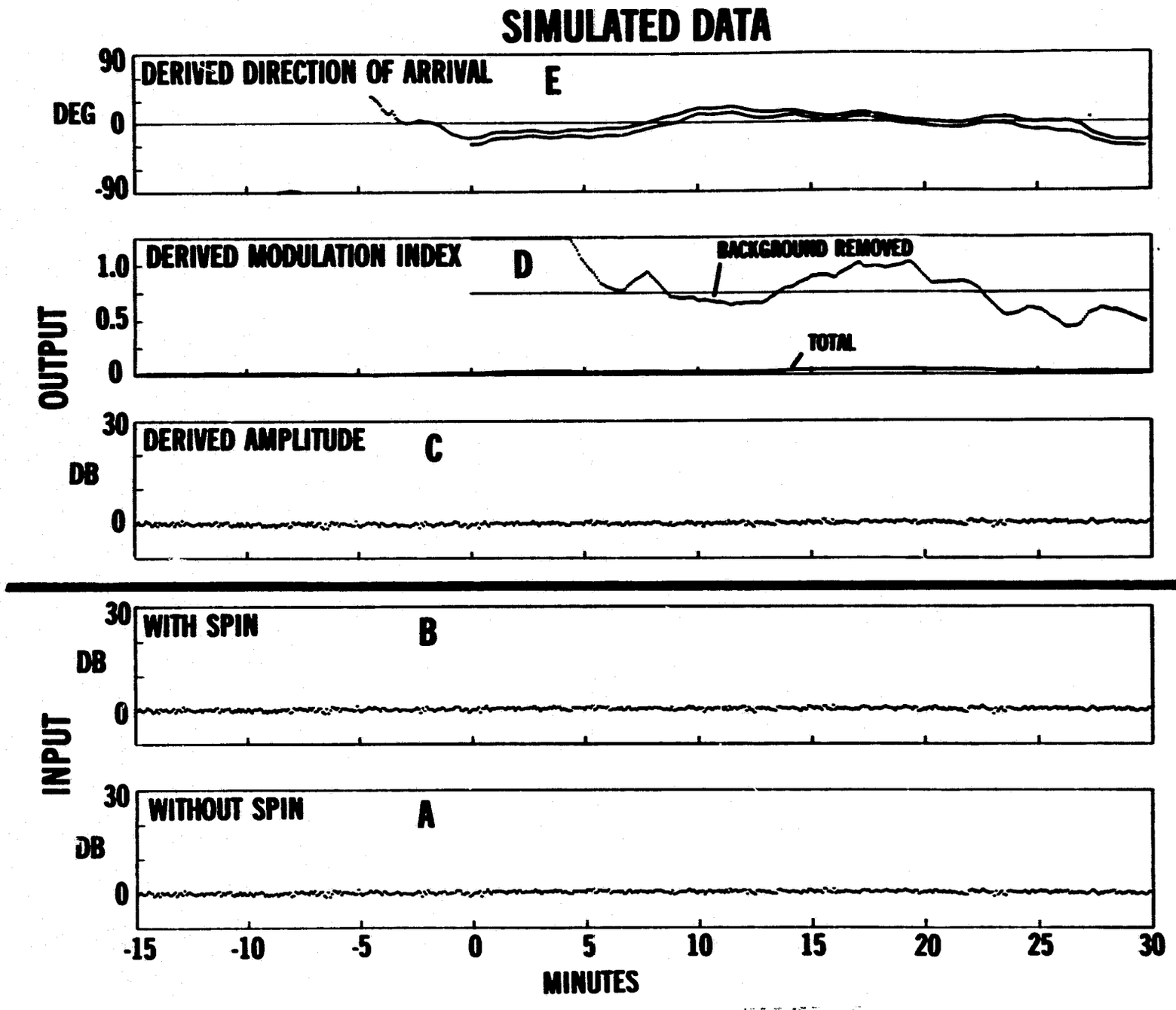
SIMULATED DATA
DERIVED DIRECTION OF ARRIVAL
E
90
DEG
0
-90
DERIVED MODULATION INDEX
D
BACKGROUND REMOVED
TOTAL
1.0
0.5
0
OUTPUT
DERIVED AMPLITUDE
C
30
DB
0
WITH SPIN
B
INPUT
WITHOUT SPIN
A
-15
-10
-5
0
5
10
15
20
25
30
MINUTES

FIGURE 5

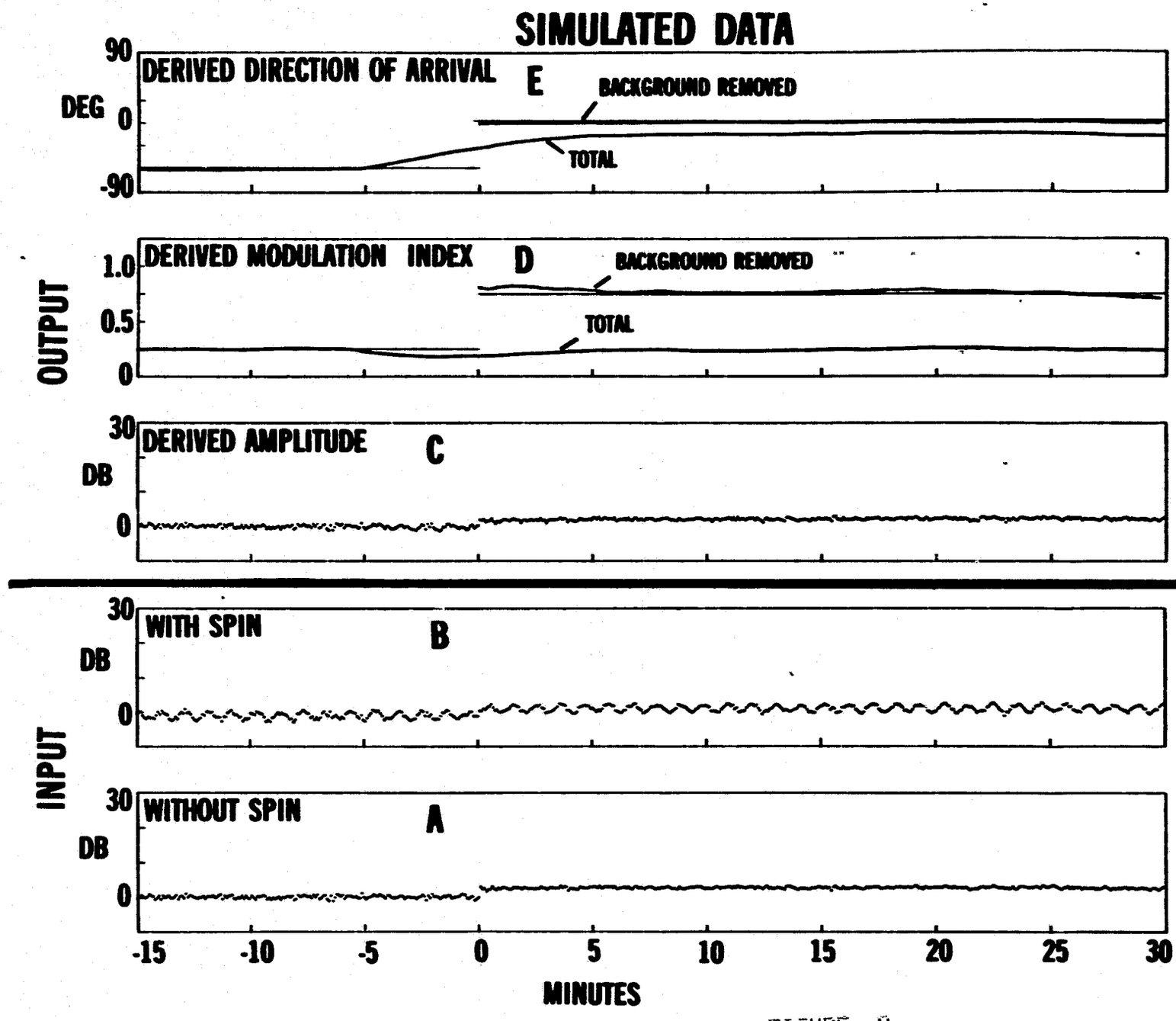
SIMULATED DATA
90
DERIVED DIRECTION OF ARRIVAL
E
BACKGROUND REMOVED
DEG
0
TOTAL
-90
DERIVED MODULATION INDEX
D
BACKGROUND REMOVED
1.0
OUTPUT
0.5
TOTAL
0
30
DERIVED AMPLITUDE
C
DB
0
30
WITH SPIN
B
DB
0
INPUT
30
WITHOUT SPIN
A
DB
0
-15
-10
-5
0
5
10
15
20
25
30
MINUTES

FIGURE 9

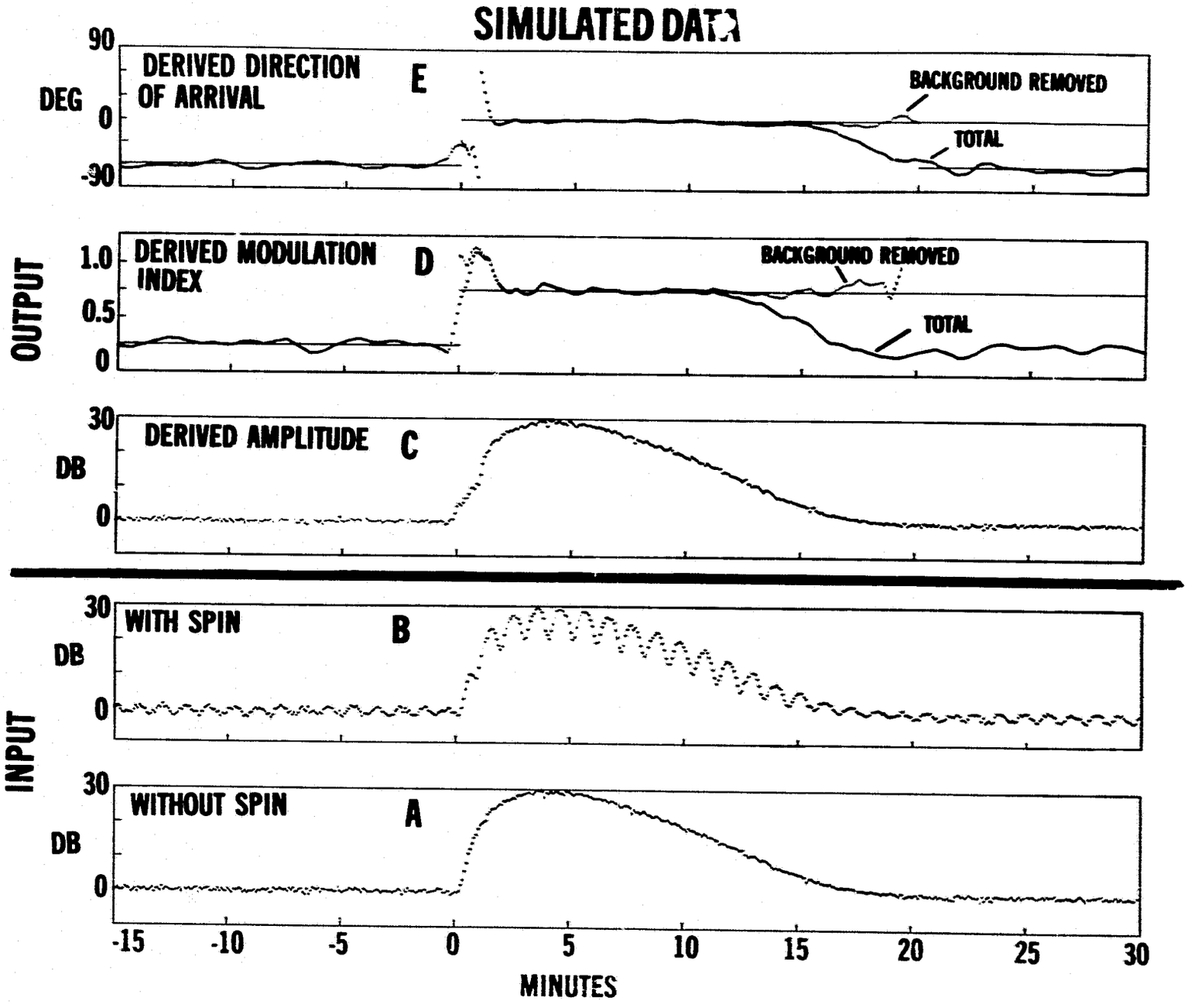
SIMULATED DATA
90
DEG
0
-90
DERIVED DIRECTION OF ARRIVAL
E
BACKGROUND REMOVED
TOTAL
OUTPUT
1.0
0.5
0
DERIVED MODULATION INDEX
D
BACKGROUND REMOVED
TOTAL
30
DB
0
DERIVED AMPLITUDE
C
INPUT
30
DB
0
WITH SPIN
B
30
DB
0
WITHOUT SPIN
A
-15
-10
-5
0
5
10
15
20
25
30
MINUTES

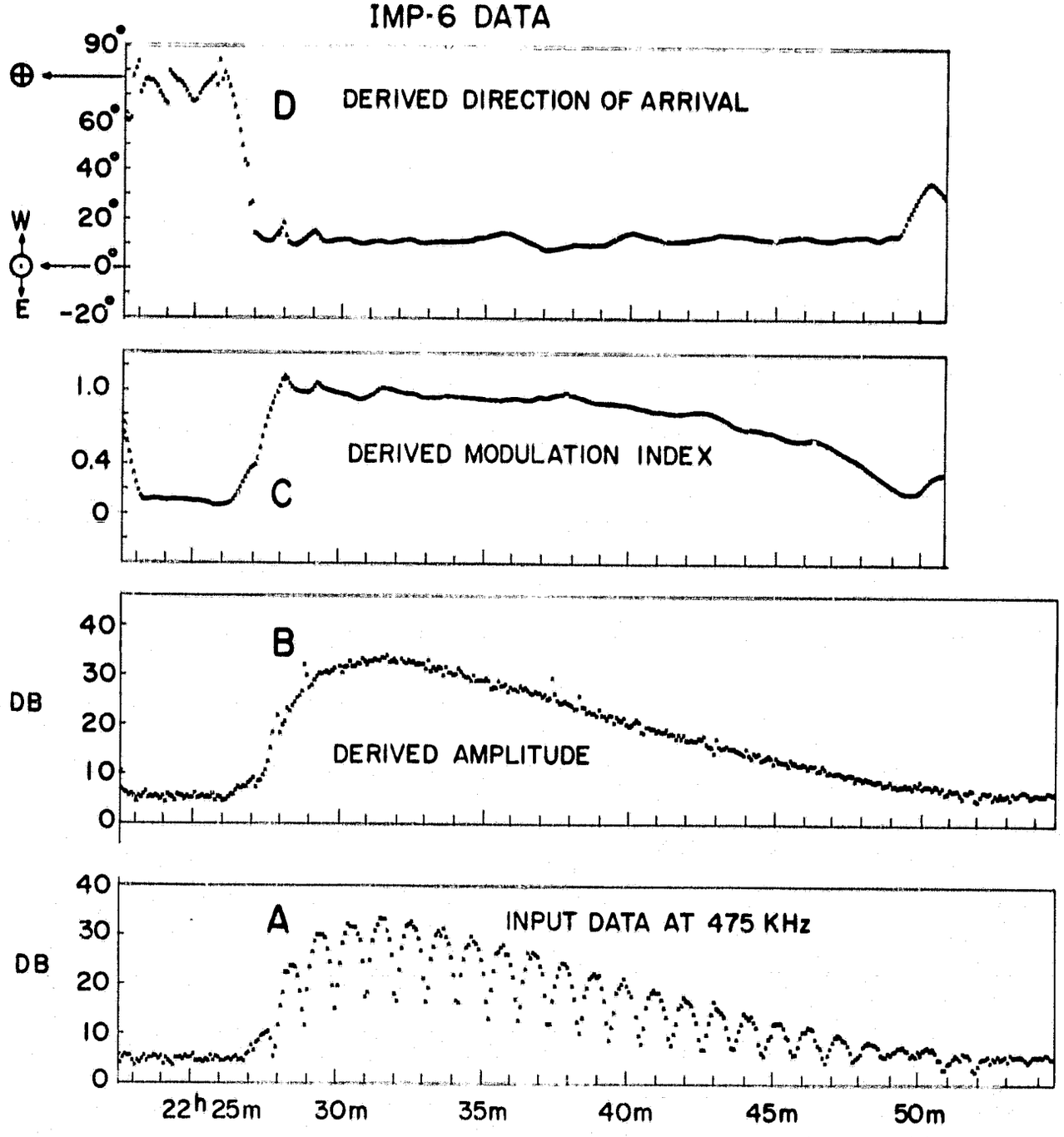
IMP-6 DATA
90°
60°
40°
20°
0°
-20°
W
E
D
DERIVED DIRECTION OF ARRIVAL
1.0
0.4
0
C
DERIVED MODULATION INDEX
40
30
20
10
0
DB
B
DERIVED AMPLITUDE
40
30
20
10
0
DB
A
INPUT DATA AT 475 KHz
22h25m
30m
35m
40m
45m
50m
U.T., 23 JUNE 1971

FIGURE 11

MEASURED ARRIVAL DIRECTIONS OF EARTH RADIO EMISSION AT 130 KHz
IMP-6 GSFC EXPERIMENT

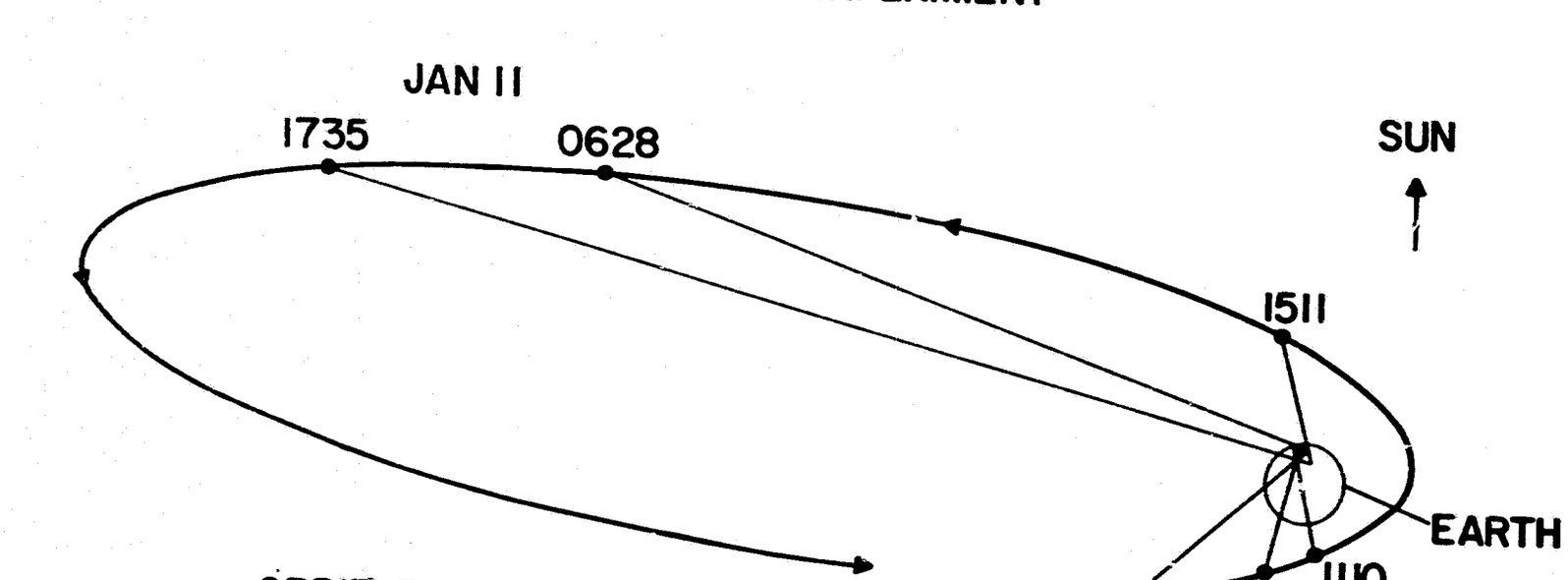

AVERAGE MID-FREQUENCY SOURCE LOCATION

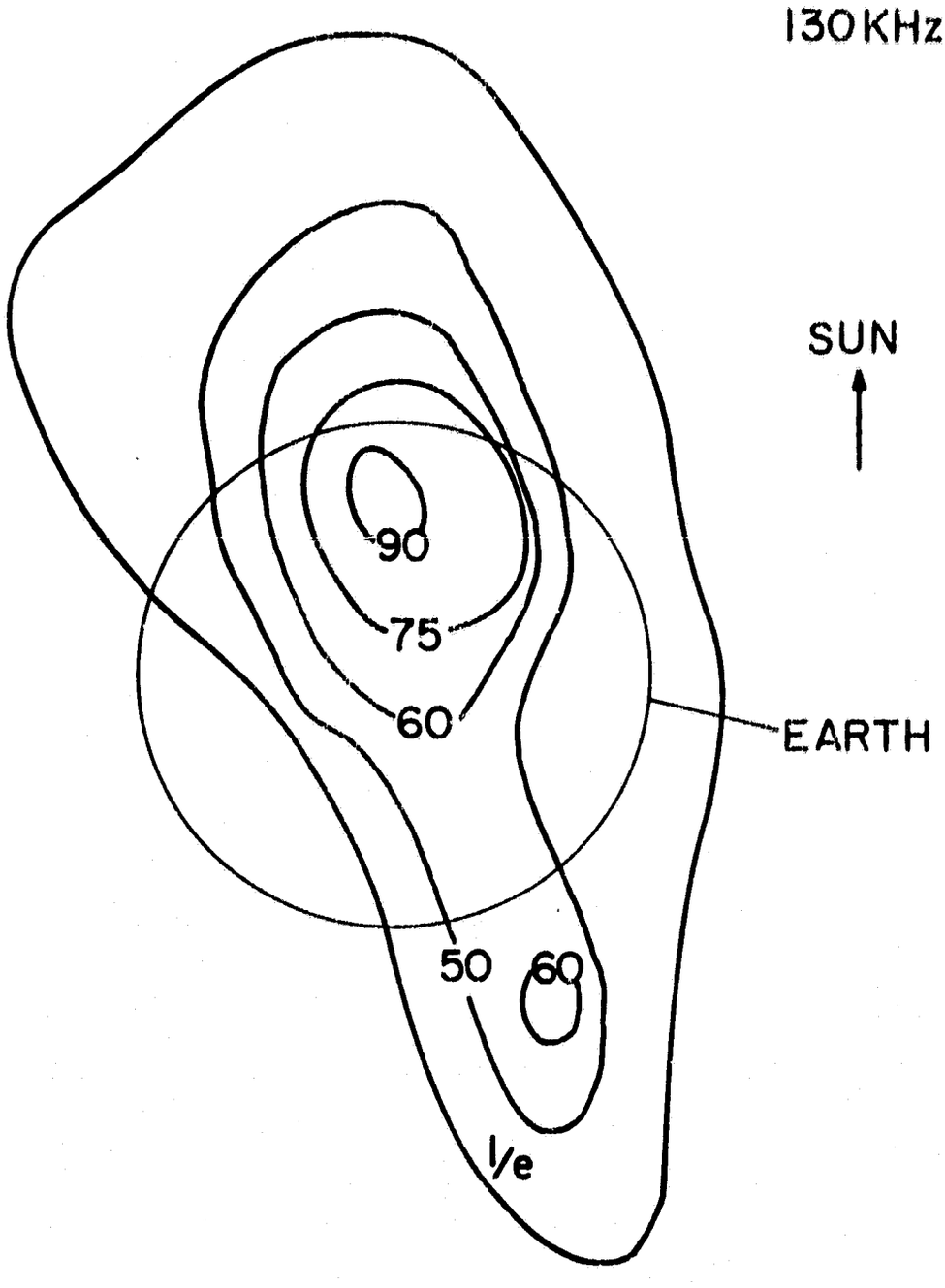

CONTOURS RELATIVE TO PEAK OCCURRENCE

FIGURE 14

IMP-6 DATA

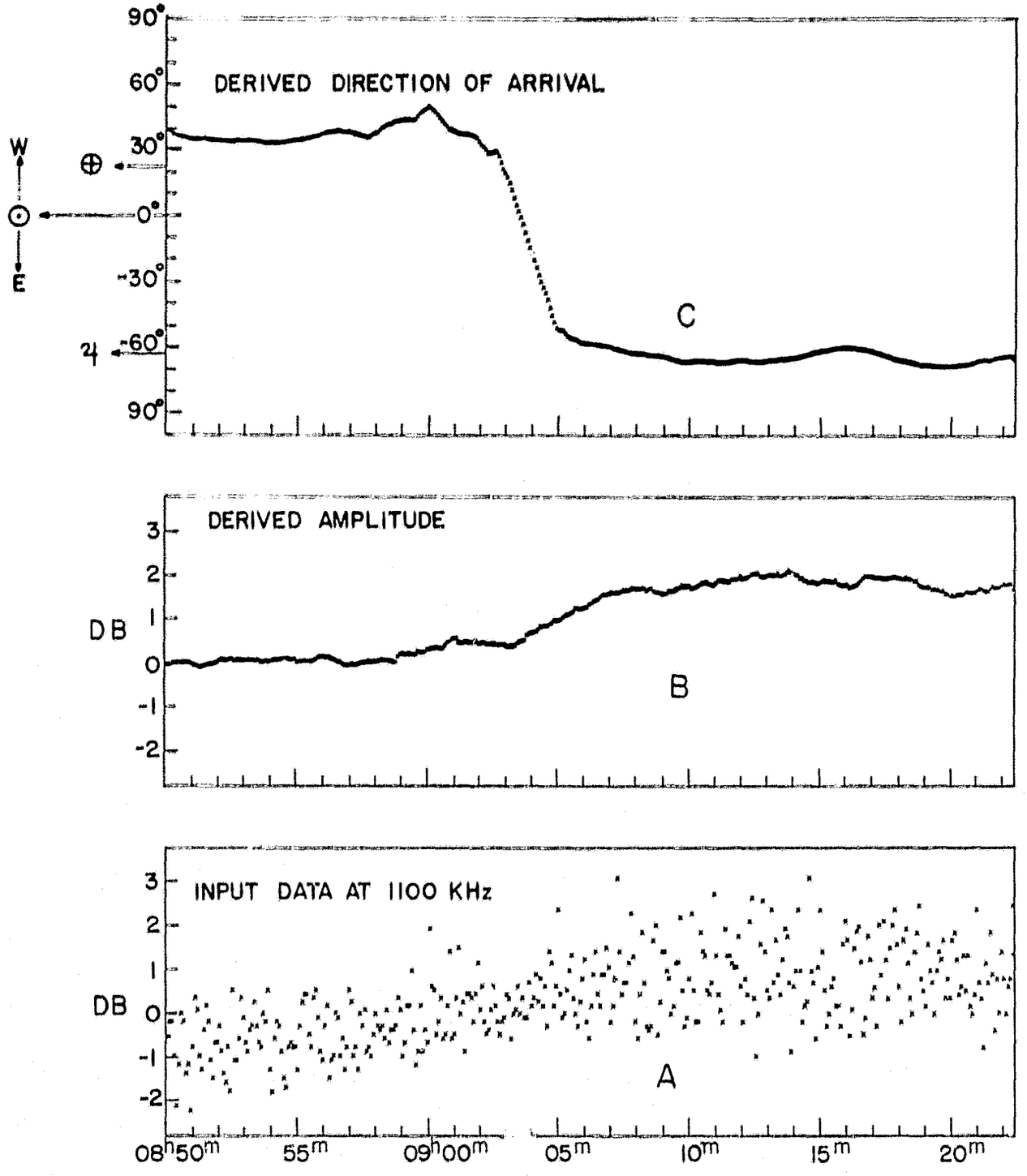

U.T., 25 APRIL 1972

BIBLIOGRAPHIC DATA SHEET

1. Report No.	2. Government Accession No.	3. Recipient's Catalog No.
TM 80598		

4. Title and Subtitle	5. Report Date
Technique to Determine Location of Radio Sources from Measurements Taken on Spinning Spacecraft	November 1979
	6. Performing Organization Code
7. Author(s)	8. Performing Organization Report No.
J. Fainberg	
9. Performing Organization Name and Address	10. Work Unit No.
NASA/GSFC Laboratory for Extraterrestrial Physics Interplanetary Physics Branch, Code 692 Greenbelt, MD 20771	11. Contract or Grant No.
	13. Type of Report and Period Covered
12. Sponsoring Agency Name and Address	Technical Memorandum
	14. Sponsoring Agency Code

15. Supplementary Notes

16. Abstract

SEE ATTACHED SHEET.

17. Key Words (Selected by Author(s))	18. Distribution Statement
Radio spin modulation technique	

19. Security Classif. (of this report)	20. Security Classif. (of this page)	21. No. of Pages	22. Price*
U	U	54	

*For sale by the National Technical Information Service, Springfield, Virginia 22151.

GSFC 25-44 (10/77)